

Review

Advancements in Doping Strategies for Enhanced Photocatalysts and Adsorbents in Environmental Remediation

Pramita Sen ¹, Praneel Bhattacharya ¹, Gargi Mukherjee ¹, Jumasri Ganguly ¹, Berochan Marik ¹,
Devyani Thapliyal ², Sarojini Verma ², George D. Verros ³, Manvendra Singh Chauhan ⁴
and Raj Kumar Arya ^{2,*}

- ¹ Department of Chemical Engineering, Heritage Institute of Technology Kolkata, Chowbaga Road, Kolkata 700107, India; pramita.sen@gmail.com or pramita.sen@heritageit.edu (P.S.); praneel.bhattacharya.che24@heritageit.edu.in (P.B.); gargi.mukherjee.che24@heritageit.edu.in (G.M.); jumasri.ganguly.che24@heritageit.edu.in (J.G.); berochan.marik.che24@heritageit.edu.in (B.M.)
- ² Department of Chemical Engineering, Dr. B.R. Ambedkar National Institute of Technology Jalandhar, Jalandhar 144011, India; devyanithapliyal5@gmail.com (D.T.); vermasarojini488@gmail.com (S.V.)
- ³ Laboratory of Polymer and Colors Chemistry and Technology, Department of Chemistry, Aristotle University of Thessaloniki, 54124 Thessaloniki, Greece; gdverros@gmail.com
- ⁴ Department of Civil Engineering, University Institute of Engineering and Technology, Babasaheb Bhimrao Ambedkar University (A Central University), VidyaVihar, Raebareli Road, Lucknow 226025, India; manvendra.hbti@gmail.com
- * Correspondence: rajaryache@gmail.com or aryark@nitj.ac.in

Abstract: Environmental pollution poses a pressing global challenge, demanding innovative solutions for effective pollutant removal. Photocatalysts, particularly titanium dioxide (TiO₂), are renowned for their catalytic prowess; however, they often require ultraviolet light for activation. Researchers had turned to doping with metals and non-metals to extend their utility into the visible spectrum. While this approach shows promise, it also presents challenges such as material stability and dopant leaching. Co-doping, involving both metals and non-metals, has emerged as a viable strategy to mitigate these limitations. In the field of adsorbents, carbon-based materials doped with nitrogen are gaining attention for their improved adsorption capabilities and CO₂/N₂ selectivity. Nitrogen doping enhances surface area and fosters interactions between acidic CO₂ molecules and basic nitrogen functionalities. The optimal combination of an ultramicroporous surface area and specific nitrogen functional groups is key to achieve high CO₂ uptake values and selectivity. The integration of photocatalysis and adsorption processes in doped materials has shown synergistic pollutant removal efficiency. Various synthesis methods, including sol-gel, co-precipitation, and hydrothermal approaches had been employed to create hybrid units of doped photocatalysts and adsorbents. While progress has been made in enhancing the performance of doped materials at the laboratory scale, challenges persist in transitioning these technologies to large-scale industrial applications. Rigorous studies are needed to investigate the impact of doping on material structure and stability, optimize process parameters, and assess performance in real-world industrial reactors. These advancements are promising for addressing environmental pollution challenges, promoting sustainability, and paving the way for a cleaner and healthier future. This manuscript provides a comprehensive overview of recent developments in doping strategies for photocatalysts and adsorbents, offering insights into the potential of these materials to revolutionize environmental remediation technologies.

Keywords: photocatalysts; adsorbents; doping; environmental remediation; pollution; co-doping; metal doping; non-metal doping; carbon-based adsorbents; nitrogen doping; visible light photocatalysis; pollutant removal; sustainability; industrial applications

1. Introduction

Metal oxide-based semiconductors play a pivotal role as photocatalysts, offering a versatile solution for various environmental and energy-related challenges. However, the



Citation: Sen, P.; Bhattacharya, P.; Mukherjee, G.; Ganguly, J.; Marik, B.; Thapliyal, D.; Verma, S.; Verros, G.D.; Chauhan, M.S.; Arya, R.K. Advancements in Doping Strategies for Enhanced Photocatalysts and Adsorbents in Environmental Remediation. *Technologies* **2023**, *11*, 144. <https://doi.org/10.3390/technologies11050144>

Academic Editor: Manoj Gupta

Received: 30 August 2023

Revised: 5 October 2023

Accepted: 9 October 2023

Published: 17 October 2023



Copyright: © 2023 by the authors. Licensee MDPI, Basel, Switzerland. This article is an open access article distributed under the terms and conditions of the Creative Commons Attribution (CC BY) license (<https://creativecommons.org/licenses/by/4.0/>).

intrinsic properties of these materials, such as their wide bandgap, had traditionally confined their utility to the ultraviolet (UV) region, limiting their efficiency in utilizing visible light. To bridge this gap, diverse strategies had been developed to harness the potential of metal oxide photocatalysts in the visible wavelength range to enhance photostability, environmental compatibility, and overall photoresponse efficiency [1,2].

One of the most promising techniques in this endeavour is the incorporation of nanoscale metal oxide particles, which significantly amplify the surface-to-volume ratio, thereby augmenting the available active sites for catalytic reactions. Among these strategies, the deliberate doping of photocatalysts with nanoparticles emerges as a highly effective approach for enhancing photoresponse efficiency. In this context, doping refers to the deliberate introduction of impurities, whether cationic or anionic, into a material to induce specific alterations in its properties. This technique had demonstrated remarkable potential in modifying the electronic structure of photocatalysts, consequently reducing their bandgap and extending their photoactivity into the visible spectrum [3].

Transition metals, including iron, manganese, copper, and nickel, and their respective oxides had been favoured choices for doping photocatalysts like TiO₂. This process had proven to be instrumental in enhancing photocatalytic efficiency under visible light irradiation by narrowing the bandgap of these catalysts [4]. However, while single-doping of TiO₂ nanocatalysts had shown promising results in improving photocatalytic efficiency, the co-doping approach with multiple transition metals can sometimes yield unfavourable outcomes due to the intricate interplay between electron–hole recombination and nanoparticle shielding effects.

In recent years, the utilization of non-metal dopants, such as nitrogen, carbon, fluorine, sulphur, and iodine, had gained prominence as an alternative doping strategy. These non-metals offer advantages, including the enhanced thermal stability of the resulting catalyst and improved performance in visible light, primarily attributed to a significant reduction in the bandgap and the suppression of electron–hole recombination processes [5].

Concurrently, adsorbents for dye removal and water treatment had witnessed a surge in the utilization of nanomaterials. These materials, encompassing polymers, carbon nanotubes, carbon nanoparticles, metals, and metal oxides, offer a substantial surface area, short intraparticle diffusion distances, multiple sorption sites, and tuneable pore sizes, making them highly effective adsorbents. Recent advancements had seen nano sorbents modified through techniques such as coating and doping to enhance their adsorption capacities [6,7].

Specifically, the introduction of alkali dopants and rare earth materials such as doping agents has proven efficacious in tailoring the adsorption properties of nanosorbents, thereby enhancing their performance.

In this paper, we embark on a comprehensive exploration of the intricate process of doping adsorbents and photocatalysts. Our objectives are as follows:

- To provide an extensive review of the methodologies employed in the synthesis of doped photocatalysts and adsorbents, encompassing the utilization of metals, metal oxides, and non-metals.
- To examine the diverse applications of doped systems, shedding light on the substantial efficiency improvements realized in doped catalysts and adsorbents when compared to their undoped counterparts.
- To scrutinize the influence of dopants on the performance of integrated adsorbent-photocatalytic units, uncovering the synergistic effects and benefits conferred by doping.
- To identify and discuss the existing limitations inherent to doping processes and propose potential strategies to overcome these limitations.

With this comprehensive overview, we aim to contribute to the broader understanding of the pivotal role played by doping in advancing the field of environmental remediation and sustainable technologies.

2. Doping of Photocatalysts with Nanoparticles

A series of key steps govern the process of photocatalysis. It commences with the absorption of photons by the catalyst, triggering the excitation of electrons, which then migrate from the valence to the conduction band. This results in the formation of electron–hole pairs, which were subsequently transported to the surface of the semiconductor catalyst. Once on the surface, a sequence of oxidation and reduction reactions takes place, generating highly reactive oxidizing species that react with adsorbed impurities, effectively decomposing them [8].

However, a significant challenge arises when using metal oxide photocatalysts like titanium dioxide (TiO_2). These materials possess a relatively wide bandgap of 3.2 eV, requiring ultraviolet (UV) radiation for activation. Unfortunately, UV radiation accounts for only a small fraction (5%) of the total solar energy, while visible radiation comprises a substantial portion (45%). Various strategies had been explored to harness the more abundant visible light, and one promising avenue involves doping photocatalysts with metal and non-metal nanoparticles. This approach offers several advantages, including enhanced light absorption, improved efficiency in separating and transferring charges, and heightened photocatalytic activity [9].

Nanoparticle doping also provides an opportunity to exert precise control over critical parameters such as particle size, shape, and distribution within the photocatalyst matrix. Additionally, it significantly increases the surface area-to-volume ratio, providing more active sites for catalytic reactions and thus enhancing overall catalytic activity [9].

The effects of nanoparticle doping are vividly illustrated in Figure 1, where it is evident that this process reduces the band gap of the photocatalyst and improves its performance. Typically, the stages involved in the nanoparticle doping of photocatalysts include the synthesis of nanoparticle dopants and their subsequent incorporation into the photocatalyst matrix. Transition metals, with their unfilled d-electron structure, play a pivotal role in facilitating the transfer of electrons from the 3d orbital of the dopant material to the conduction band of TiO_2 . This enables the accommodation of a greater number of photogenerated electrons and holes, effectively shifting TiO_2 's response towards visible wavelengths [8–10].

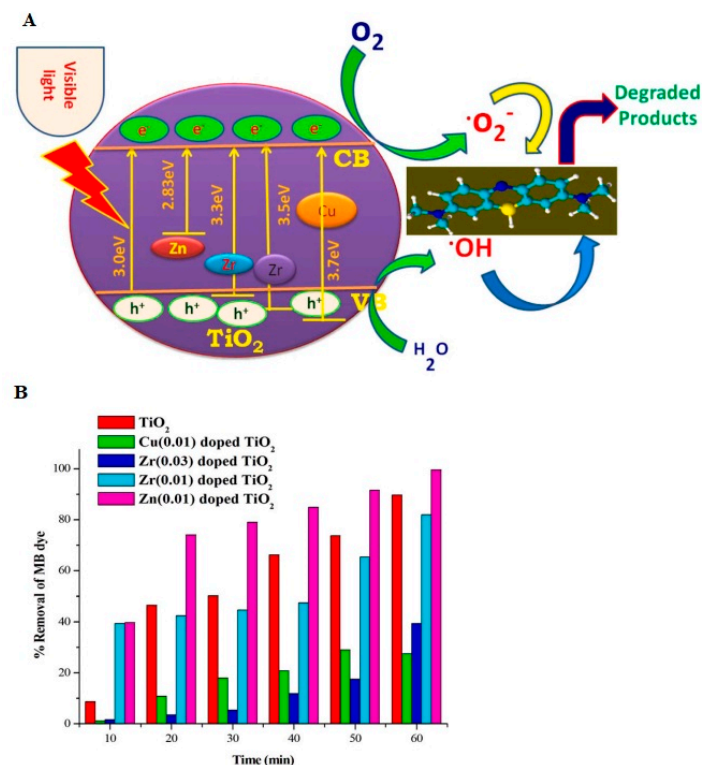


Figure 1. (A) Bandgap energy diagram of pure titania, copper, zirconium, and zinc-doped titania. (B) Percentage of dye removal with undoped and doped TiO_2 (Copyright permission from [11]).

Among the metal oxides used as photocatalysts, titanium dioxide (TiO_2), zinc oxide (ZnO), tin dioxide (SnO_2), and cerium dioxide (CeO_2) were preferred due to their harmonious combination of electronic structure, light absorption capacity, charge transport characteristics, and durability. Moreover, additional metal oxides, including barium titanate (BaTiO_3), strontium titanate (SrTiO_3), sodium tantalate (NaTaO_3), barium tantalate (BaTaO_3), sodium niobate (NaNbO_3), hafnium dioxide (HfO_2), and zinc ferrite (ZnFe_2O_4), had shown excellent progress as photocatalysts [9].

2.1. Doping with Metal and Metal Oxides

Doping with metals and metal oxides is a pivotal strategy used in photocatalysis to boost the performance of photocatalytic materials like titanium dioxide (TiO_2). This technique involves introducing specific types of metals or their oxides into the photocatalyst's structure, fundamentally altering its physical and chemical properties [12]. These modifications often enhance light absorption, charge separation, and overall photocatalytic activity.

A variety of techniques were employed to introduce these metal dopants into photocatalytic materials.

2.1.1. Sol–Gel Method

The sol–gel technique is a widely adopted approach. It starts with the creation of a homogeneous solution containing metal precursors. This solution undergoes a process called condensation, leading to the formation of a gel. Subsequent drying removes the solvent, yielding metal-doped nanoparticles [13–19]. For example, Neodymium (Nd) doping in TiO_2 nanoparticles was accomplished by mixing solutions of Neodymium (III) acetate dehydrate in isopropyl alcohol with a titanium isopropoxide solution in alcohol. The addition of acetic acid and pH adjustment completed the hydrolysis process, resulting in transparent sols. After aging, thorough washing, centrifugation, drying, and annealing, Nd-doped TiO_2 nanoparticles were produced. This process enhances the photocatalytic removal of dyes and pollutants under solar light [19]. Similar methods had been applied to Neodymium doping with variations [17]. Rare earth elements other than Neodymium—namely, Lanthanum (La), Europium (Eu), and Gadolinium (Gd)—had also been used for doping TiO_2 to improve the photocatalytic performance of TiO_2 , and the doped photocatalysts prepared by the sol–gel method were successfully applied for pollutant/dye removal [20,21]. Apart from TiO_2 , rare earth element-doped ZnO nanoparticles synthesized by the sol–gel method had been used extensively in dye degradation [22–25]. In recent studies, the sol–gel method was employed to synthesize nickel-doped ZnO nanoparticles to be used as photocatalysts with 94% dye degradation ability [26] and to prepare cerium-doped $\text{ZnO}:\text{TiO}_2$ nanocomposite-based photocatalysts for dye degradation and antibiotic removal [27]. Europium (Eu)-doped nanocomposites of $\text{ZnO}-\text{SnO}_2$, synthesized by the sol–gel method, exhibited enhanced dye degradation efficiency due to the formation of Z-scheme heterojunctions in the presence of the Eu ions [28].

The synergistic enhancement of CO_2 photo-reduction and selectivity towards CH_4 using bismuth-doped TiO_2 had been observed by earlier researchers [29]. A bismuth-based TiO_2 nanocatalyst was prepared by the sol–gel method. Furthermore, photo-deposited platinum on the catalyst surface had been effectively used as an electron-trapping agent with the ability to extract the electrons trapped on the surface of TiO_2 in a few picoseconds.

TiO_2 photocatalysts doped with iron [30] and co-doped with manganese and boron [31] had been synthesized with enhanced structural and photocatalytic properties using the sol–gel method for dye removal. Silver-doped TiO_2 nanoparticles had been widely used as photocatalysts due to the following reasons: firstly, their enhanced photocatalytic efficiency in the visible light induced by the surface plasmon resonance effect; secondly, the creation of a Schottky barrier at the TiO_2 interface to trap electrons from the conduction band and transfer them to oxygen, thereby preventing electron–hole recombination; and thirdly, the enhanced antibacterial properties of silver, which were another essential feature for its selection as a doping agent [8]. Several techniques had been used to synthesize silver-doped

TiO₂ nanoparticles, including sol–gel, hydro/solvothermal, photo-deposition, chemical reduction, impregnation, and co-precipitation. The sol–gel route had been used to prepare silver-doped TiO₂ nanopowder via dropwise addition of an aqueous solution of silver nitrate to a mixture of TiO₂ in acetic acid, resulting in gel formation. In one instance, the gel was air dried and annealed to yield the photocatalyst in nanopowder form to be employed for dye removal [32]. In another instance, silver-loaded TiO₂-ZnO thin films were prepared on glass substrates using the sol–gel method. A TiO₂ precursor solution was prepared by mixing titanium isopropoxide, acetic acid, propanol, and water. ZnO sol was subjected to 48 h of aging before mixing with the TiO₂ sol, and doping was achieved by adding a silver nitrate solution of different concentrations to the mixed sol. The pretreated glass substrates were dipped in the silver-doped sols, dried, and treated thermally [33].

In a recent study, cerium-doped ZnO/TiO₂ nanospheres were synthesized for a photocatalytic degradation of dye and levofloxacin in visible light where ZnO and TiO₂ sols were initially mixed, followed by adding the precursor solution of the dopant cerium and stirring for 3 h. The addition of NaOH solution to the doped solution was followed by centrifugation, washing, drying, grinding the precipitate, and sintering them at 500 °C for 3 h to yield the final photocatalyst [27].

2.1.2. Solvo/Hydrothermal Treatment

Hydrothermal methods were employed to synthesize photocatalysts under high-temperature and high-pressure conditions in an aqueous environment. This technique allows for precise control over particle size and structure. Researchers used hydrothermal treatment to prepare various doped photocatalysts, including Nd-doped TiO₂ [20,21]. Researchers attempted to modify TiO₂ by adsorbing photosensitive molecules, such as hetero-poly(phosphotungstic acid) (HPA), on its surface. Nd-doped TiO₂ was prepared through hydrothermal treatment by adding the dopant neodymium salt to a titanium isopropoxide solution, followed by distilled water to induce precipitate formation [16]. Another recent study used hydrothermal treatment to prepare copper-doped mesoporous TiO₂. A solution of polyvinyl alcohol in boiling water was mixed with titanium isopropoxide in acetic acid, followed by ultrasonication and calcination. Copper nanoparticles of different weight percentages were added to prepare the doped photocatalyst [34]. Magnesium-doped SnO₂ nanoparticles with enhanced photocatalytic activity and catalyst reusability were prepared using a hydrothermal technique [35].

This versatile one-step hydrothermal method creates nanocomposites of metal-doped titanium oxide–graphene oxide. It involves mixing graphene oxide with metal and titanium precursors and subjecting the mixture to hydrothermal treatment. This results in composite powders containing various metal dopants, such as silver, copper, and palladium [36]. A one-step hydrothermal method had recently been used for preparing iron-doped Bi₂O₂CO₃ photocatalysts with FeO_x nanoparticles deposited on the photocatalyst. Here, a combination of doping and co-catalyst addition was employed to enhance the photocatalytic degradation ability of Bi₂O₂CO₃ to a maximum value in visible range [37].

2.1.3. Pulsed Laser Ablation in Liquid (PLAL)

PLAL technology offers a novel approach to producing metal-doped nanoparticles. It involves the laser-induced ablation of a target material submerged in a liquid medium. The poor solubility of dopants in the photocatalyst matrix was a major factor hindering the achievement of high photocatalytic activity and can be overcome using plasma-assisted laser ablation techniques. This method had been utilized to generate Nd-doped ZnO nanoparticles [38,39], allowing for precise control over dopant incorporation. In the double pulse laser ablation technique, a zinc plate serving as the target was added to the neodymium salt solution, followed by the irradiation of the target with a pulsed laser for 10 nanoseconds, resulting in the formation of plasma near the target. The doped colloidal nanoparticles were further subjected to laser modifications [38]. In another instance, the doping efficiency of the solvent during a laser ablation of Gd₂O₃ with Europium was tested,

where the doping concentration was found to be proportional to the initial concentration of the dopant in an aqueous solution over two orders of magnitude. The mechanism of laser-ablated doping was revealed [39].

2.1.4. Flame Spray Pyrolysis

Flame spray pyrolysis (FSP) is another method employed for preparing metal oxide-doped photocatalysts. In this process, precursors were dissolved in alcohol and introduced into a reactor. The combustion of methane and oxygen generates a flame, evaporating the precursors and forming doped nanoparticles. This technique produces uniform and well-defined nanoparticles, such as ZnO nanoparticles doped with WO_3 [40]. In another instance, single nozzle-based FSP had been used to synthesise lanthanum-doped perovskite SrTiO_3 for hydrogen production. In contrast, double nozzle FSP was used for creating a heterojunction between CuO and lanthanum-doped SrTiO_3 for the selective photocatalytic production of CH_4 from $\text{H}_2\text{O}/\text{CH}_3\text{OH}$. In the dual nozzle FSP, two asymmetrically placed FSP nozzles operate in tandem—the left one used for producing Lanthanum-doped SrTiO_3 nanomaterial and the right one for CuO nanoparticles. This was followed by depositing the nanoparticles and binder on a glass microfiber filter with the aid of a vacuum pump and scrubbing the nanoparticles from the filter [41].

2.1.5. Chemical Precipitation and Co-Precipitation

The synthesis of tin-doped zinc nanoparticles with the chemical precipitation method was carried out by adding potassium hydroxide solution dropwise to an aqueous solution of tin chloride dihydrate and zinc acetate dihydrate. The purification of white precipitate followed by air-drying at $100\text{ }^\circ\text{C}$ for 6 h and annealing at $300\text{ }^\circ\text{C}$ for 3 h in a muffle furnace resulted in the final product [42]. In another instance, the co-precipitation method synthesised iron-doped ZnO nanoparticles [43]. Here, zinc acetate dihydrate, the precursor of ZnO nanoparticles, and ferric chloride, the precursor of iron, was dissolved in water, followed by the addition of NaOH solution to maintain an alkaline pH. The mixture was heated at $85\text{ }^\circ\text{C}$ for 2 h, cooled, and kept for 24 h. The precipitate obtained was washed, dried, and annealed at $400\text{ }^\circ\text{C}$ to obtain the final product. Recent studies reported green synthesis methods for synthesizing ZnO/ WO_3 nanocomposites for the photocatalytic removal of organic pollutants [44]. A comparative study was conducted between nickel-doped Co_3O_4 and bimetal-doped Co_3O_4 photocatalysts to identify the best combination of dopants and photocatalysts during visible light dye degradation. The two dopant metals other than nickel were copper and cadmium. The Cadmium–nickel bi-doped photocatalyst exhibited the greatest photocatalytic activity of 93% [45].

Figure 2 presents schematic diagrams illustrating the synthesis of metal-doped TiO_2 through different routes, showcasing the adaptability and potential of these methods. Metal and metal oxide doping continue to be at the forefront of research in the field of photocatalysis, driving innovations and improvements in performance across a wide range of applications.

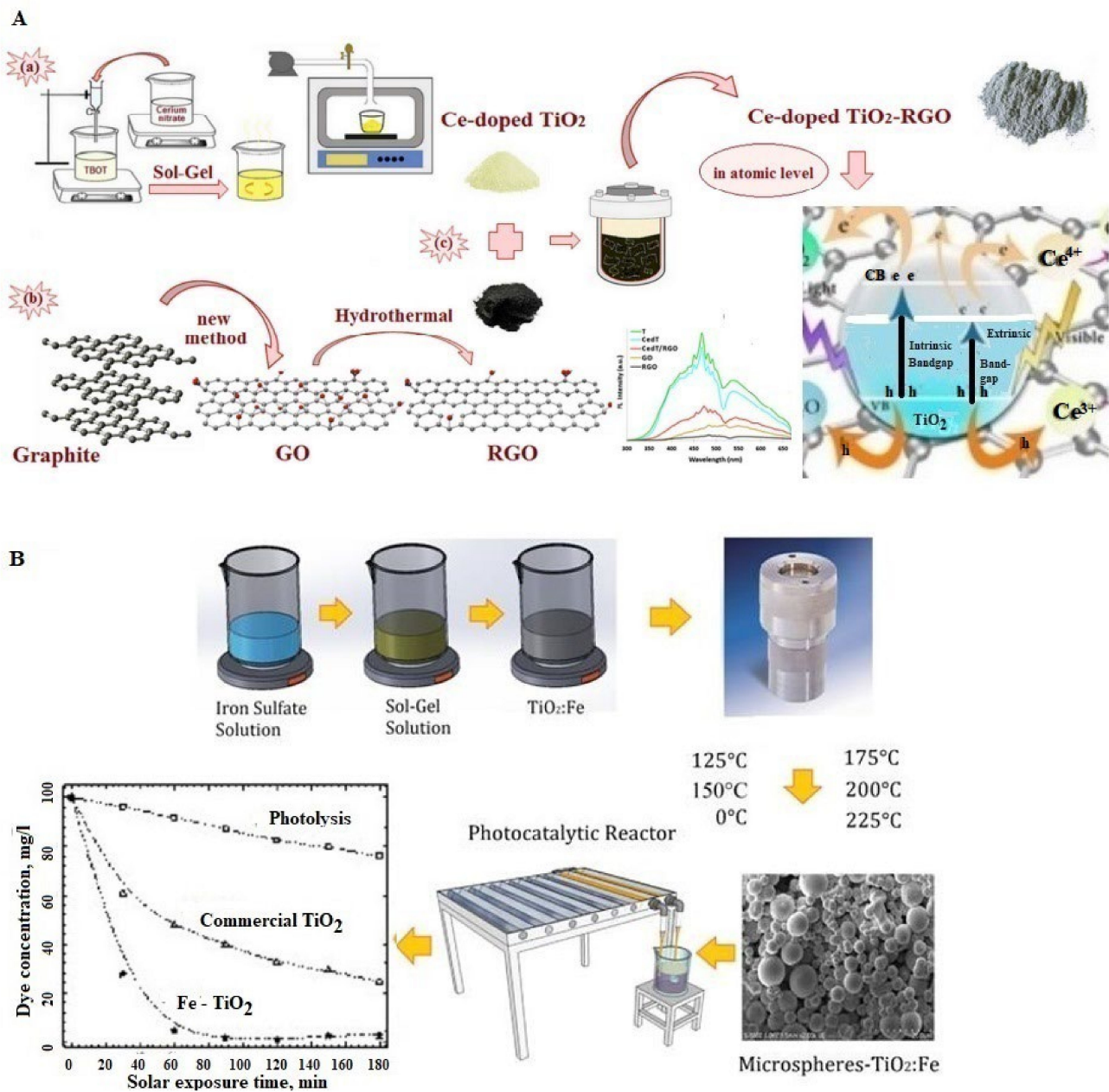


Figure 2. (A) Schematic diagram showing the (a) synthesis of cerium-doped TiO₂, (b) reduced graphene oxide, and (c) Cerium-doped TiO₂-reduced graphene oxide composite (Copyright from [46]). (B) Schematic diagram of iron-doped TiO₂ synthesis via hydrothermal treatment followed by dye degradation (Copyright from [47]).

2.1.6. Recent Progress in Metal-Doped Photocatalysts

Recently, a combination of two or more techniques had been used to prepare photocatalysts with several enhanced properties, including optical, photocatalytic properties, UV-induced wettability, and self-cleaning effects. A recent study used a combination of sol-gel and spin coating methods for doping copper in zinc oxide thin films. The precursor solutions for zinc and copper were dissolved in a mixture of solvent and stabilizer and stirred at 60 °C. The coating sol, thus obtained, was kept in the dark for a day and spin-coated at 2000 rpm on a glass substrate for 30 s. The spin coating was followed by drying at 180 °C, and the processes of spin coating and drying were repeated multiple times. Annealing was performed at 500 °C for 2 h, forming copper-doped zinc oxide film with enhanced photocatalytic, super-hydrophilic, and self-cleaning properties [48].

Copper-doped nickel oxide nanoparticles with a new morphology and modified band gap were synthesized by combining co-precipitation and calcination [49]. The calcination temperatures affected the morphologies of the doped photocatalyst and surface areas. In a recent study, tin-doped TiO₂ nanoparticles were synthesized by a sol-gel route followed by calcination at various temperatures from 450–750 °C. The optimum formulations of tin-doped TiO₂ were screen printed and annealed at 500 °C. A dispersion of the synthesized nanoparticles in 2-propanol, α -terpeniol, and ethyl cellulose was prepared, followed by the incorporation of additives, and the mixture was homogenized to produce a paste which was screen printed on a glass slide using a hard square edge polyurethane squeegee and 400 meshcount screens [50]

A green synthesis method involving a microwave-assisted combustion technique with *Tamarindus indica* seed extract as fuel was used to synthesise Ni-doped magnesium ferrite nanoparticles with a spinel cubic structure for use as visible range photocatalysts for dye degradation [51]. The sol-gel auto-combustion method had been used for synthesizing metal-doped nano cubic spinel ferrite-based photocatalysts for wastewater treatment [52,53]

Considerable enhancement of the photocatalytic activity of TiO₂ during hydrogen production had been achieved by using two-dimensional transition metal-based carbonitrides, also known as MXenes, as cocatalysts. MXene offers the unique advantage of possessing a layered structure, excellent conductivity, excellent exposure to metallic sites, and tuneable electronic structures. Electrostatic self-assembly and photoreduction processes were used to prepare the Ag/Ti₃C₂/TiO₂ nanocomposites for photocatalytic hydrogen production. The scheme for the synthesis process is illustrated in Figure 3 [54].

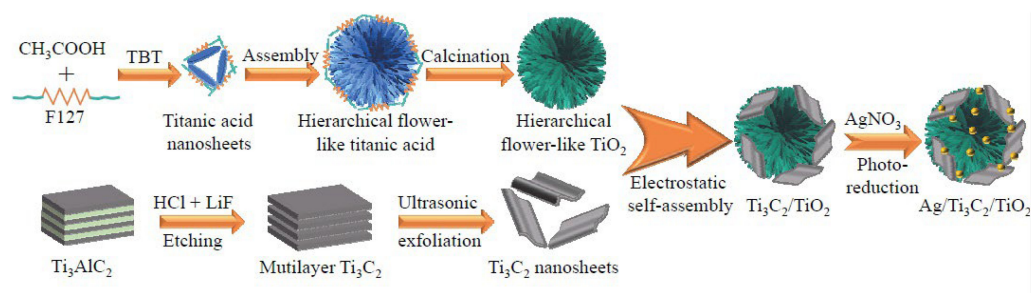


Figure 3. Schematic for preparation of Ag/Ti₃C₂/TiO₂ nanocomposites (Copyright permission from [54]).

The solar-driven photocatalytic reduction of CO₂ to CH₄ and CO is a newly evolved, promising strategy for addressing energy challenges and environmental concerns. In this respect, metal-organic frameworks had emerged as promising photocatalytic materials, with their organic ligands serving as light-harvesting centres, activating the metal cluster nodes. However, MOFs suffer from limitations—namely, poor charge separation, low conductivity values and poor migration efficiency. In a recent study, the drawbacks were overcome by synthesising a durable hybrid cobalt-based MOF/Cu₂O composite containing a p–n heterojunction for carrying out solar-driven CO₂ photoreduction with increased efficiency. An ultrasonicated aqueous solution of MOF was mixed with CuCl₂·2H₂O and NaOH solutions, followed by a dropwise addition of ascorbic acid solution. The resulting suspension was centrifuged and vacuumdried to yield a fine composite powder [55]. In another study, the facile hydrothermal method was used to fabricate azobenzene tetracarboxylic acid-based MOF for the effective photocatalytic reduction of CO₂ to CH₄, along with high CH₄ selectivity [56]. The solvothermal method was recently used to incorporate a rhodamine dye molecule into a zirconium-based MOF framework to fabricate a dye-sensitized photocatalyst for CO₂ reduction. Anchoring the dye molecule into MOF-based semiconductors expands the light absorption range of the photocatalyst and initiates the transfer of electrons from the excited dye molecule to the MOF. The composite was prepared via reaction of the dye and the MOF in water at 120 °C for 24 h. After cooling to room

temperature, precipitates were centrifuged and washed thoroughly to remove additional dyes, followed by vacuum drying [57].

The construction of a heterojunction ensures enhanced carrier mobility and improved the photocatalytic performance of the catalysts. However, interface defects and poor energy levels can lead to interface recombination, leading to a loss in photocatalytic performance. Reduction in interfacial recombination had been carried out by adjusting the band alignment in the existing photocatalyst. The cliff-like conduction band offset (CBO) in CuSbS₂ (CAS)/ZnO was modified by coupling another material, CdS, to form spike-like CBO, resulting in a reduced interface combination rate and increased photocatalytic efficiency. The CAS–ZnO–CdS heterojunction prepared by the microwave-assisted method produced a hydrogen evolution of 140.45 μmol/g after 4 h of illumination [58]. A combination of solvothermal and electrospinning technology was used for preparing CuBi₂O₄–Bi₂WO₆ nanofibres with Z scheme heterojunction with a 90% degradation efficiency of tetracycline hydrochloride [59].

Single-atom catalysts performed excellently due to the uniform adsorption of reactants/intermediates on each active site and avoidance of multiple adsorptions. They were highly selective for reactions—namely, hydrogenation, electrocatalysis, and oxidation—and exhibit high activity. Nitrogen-doped graphene (NG) material with N as the Lewis base binds strongly to the Lewis acid, namely, single-atom metal centre. It provided a stable, coordinated environment for the single metal atom. A recent study used a precursor dilution strategy to prepare a copper/nickel dispersed poly(tetraphenyl porphyrin) through Friedel Crafts alkylation, and it was deposited on modified TiO₂ microspheres. The atomically dispersed Cu–N₄ and Ni–N₄ complexed with NG were subsequently synthesized via calcination at 800 °C [60]. The desulphurization of dibenzothiophene using the bimetallic single-atom catalyst was 100%, with a total metal loading of 0.1 wt% for both metals. A narrow band gap semiconductor (~1.5 eV), CuInS₂, had been used in photocatalytic hydrogen evolution, pollutant degradation, and CO₂ reduction due to its strong response under visible light and excellent stability. A combination of hydrothermal and calcination methods had been used for fabricating a boron-doped TiO₂/CuInS₂ Z scheme heterojunction yielding 21.39 μmol/g/h of CO and 4.83 μmol/g/h of CH₄ during a photocatalytic CO₂ reduction with no significant reduction in yield after three cycles. The yield of gases was 10 and 13 times higher than the standalone TiO₂ and boron-doped TiO₂. The oxygen-rich species and Ti³⁺ introduced by boron doping acted as electron traps for preventing the recombination of the photogenerated carriers, and heterojunction hastened the separation of carriers, retained electrons and holes, and improved visible light absorption [61]. The combination of hydrothermal and calcination methods used for the synthesis of MXene-based catalysts is demonstrated in Figure 3.

2.2. Photocatalysts Doped with Non-Metals

Non-metal doping had gained substantial attention in photocatalysis due to its potential advantages over metal doping. Non-metal elements—such as carbon, nitrogen, and sulphur—offer unique opportunities for modifying photocatalytic materials without some of the drawbacks associated with metal dopants, such as increased thermal instability, poor dopant solubility, secondary phase formation, and phase transformations [47]. This section explores various non-metal doping strategies and their implications for enhancing photocatalytic performance.

Carbon doping of TiO₂ nanoparticles had been explored as an approach to extend their photocatalytic activity into the visible light range. This was typically achieved using the sol–gel method, incorporating a stabilizing agent and a titanium tetra-isopropoxide precursor. Interactions among the doped carbon, titanium, and oxygen atoms within the TiO₂ lattice lead to a reduction in the band gap energy. By adjusting the concentrations of the stabilizing agent and the carbon dopant, researchers finely tuned the band gap energy, thereby facilitating photocatalytic reactions in the visible light spectrum. Additionally, vari-

ations in dopant and stabilizing agent concentrations allow for favourable microstructure modifications, further optimizing photocatalytic performance.

Ionic liquids had proven to be effective sources of co-dopants, including carbon and nitrogen, for mesoporous titania nanoparticles. Co-doping with carbon and nitrogen can be achieved by introducing appropriate amounts of ionic liquid into solutions containing titanium isopropoxide in ethanol. This process involves evaporation-assisted self-assembly and subsequent calcination [62]. Alternatively, several mechanical and chemical methods, such as ball milling, sol–gel synthesis, sputtering, solvothermal and hydrothermal processes, and the direct hydrolysis of salts, had been employed to introduce nitrogen into the titania lattice. Nitrogen sources for doping include urea, thiourea, nitrogen dioxide, ammonia, and triethylamine [63].

One innovative application of non-metal doping involves the development of nanocomposites composed of TiO_2 and reduced graphene oxide doped with nitrogen. These nanocomposites had shown excellent results in carbon dioxide (CO_2) photoreduction. The synthesis of such nanocomposites typically involves a urea-assisted single-step hydrothermal method. In this process, graphene oxide was dispersed in an aqueous ethanol solution, followed by the addition of urea and TiO_2 . The mixture was subjected to high-temperature hydrothermal treatment, forming solid nanocomposites with exceptional photocatalytic properties for CO_2 conversion [64]. The solvothermal synthesis of nitrogen-doped TiO_2 and Fe_2O_3 nanocomposites yielded photocatalysts with enhanced activity owing to the formation of a heterojunction between nitrogen-doped TiO_2 and Fe_2O_3 . The nanocomposite absorbed light at a higher rate compared to the TiO_2 alone and resulted in the nearly complete oxidation of methanol [65].

Solvent-based multi-doping strategies had also been explored, aiming to enhance the optoelectronic properties of TiO_2 . These strategies involve doping TiO_2 with non-metals (nitrogen, carbon, and sulphur) and metals (e.g., iron) using the sol–gel synthesis method. Titanium isopropoxide was typically added to an aqueous solution containing thiourea and iron chloride. Stirring the solution for an extended period, followed by aging, air-drying, grinding, and calcination yielded multi-doped TiO_2 materials with tailored properties [66].

Another noteworthy approach incorporated fluorine-doped graphene as a supporting matrix for the synthesis of gadolinium orthovanadate nanoparticle-based photocatalysts. In this process, fluorine-doped graphene was prepared by mixing graphene and sodium fluoride in water, followed by sonication and shaking. The resulting fluorine-doped graphene was then dispersed in water, and gadolinium nitrate and polyethylene glycol were added to create a homogeneous dispersion of the photocatalyst on the support. This approach offered intriguing possibilities for designing advanced photocatalytic materials [67].

Figure 4 provides a comprehensive visual representation of the intricate synthesis process involved in creating nitrogen-doped mesoporous TiO_2 ($\text{TiO}_2\text{-N}$), a highly advanced photocatalytic material with promising applications. The illustration delineates critical elements of the synthesis, starting by using various chemical reagents crucial for introducing nitrogen dopants into the TiO_2 structure. The depiction of a controlled reaction vessel underscores the importance of maintaining precise conditions during synthesis. The source of nitrogen dopants, likely involving ammonia or similar compounds, is highlighted, emphasizing its role in achieving successful nitrogen doping. Additionally, the figure elucidates the mesoporous structure of TiO_2 , essential for maximizing the material's surface area, thereby enhancing photocatalytic activity. The heart of the illustration lies in illustrating how nitrogen atoms were integrated into the TiO_2 lattice, a fundamental alteration that extended the material's photocatalytic capabilities into the visible light spectrum. Overall, Figure 4 offers valuable insights into synthesising nitrogen-doped mesoporous TiO_2 . It highlights controlled chemical reactions as the key to its advanced properties, particularly its enhanced ability to harness solar energy and address environmental challenges through advanced photocatalysis.

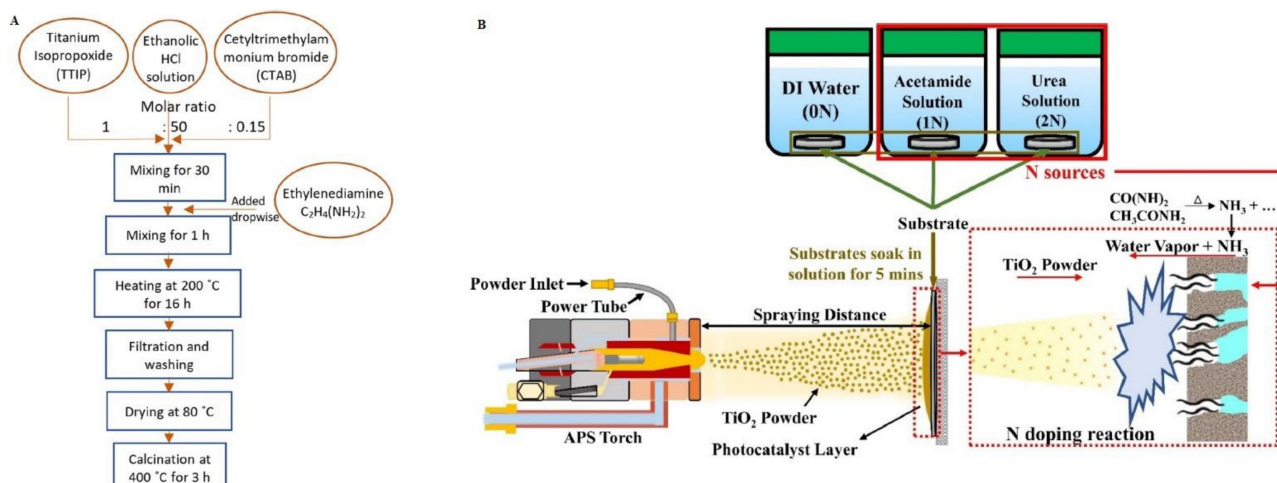


Figure 4. (A) Synthesis of N-doped mesoporous TiO₂ (Copyright permission from [68]). (B) Synthesis of N-doped reduced TiO₂ using atmospheric plasma spraying (APS) (Copyright permission from [69]).

This section underscores the diverse strategies employed to introduce non-metal dopants into photocatalytic materials, highlighting their potential to enhance performance and broaden the scope of photocatalysis.

Nitrogen-doped TiO₂ exhibited boosted visible light absorption due to the shifting of 2p orbital levels. In a recent study, Ag/AgCl/N-doped TiO₂ photocatalysts had been synthesized for achieving high ammonia conversion during photocatalytic ammonia oxidation and significant N₂ selectivity compared to NO_x due to a change in the reaction pathway [70]. A combined sol-gel and photo deposition method was used for preparing the catalyst. In another instance, the stability of N-doped carbon material in peroxydisulphate-based Fenton reactions was enhanced by synthesizing N-doped carbon spheres with TiO₂ nanoparticles supported on the inner surface of the hollow spheres [71]. Direct electron transfer (DET)-based non-radical activation of persulfates utilized the N-doped carbon material as electron transport conductors and reduced the persulfates without being oxidized. To achieve this, N-doped carbon was deposited on TiO₂ nanoparticle-wrapped SiO₂ via chemical vapour deposition followed by alkali etching, which resulted in the generation of the TiO₂-incorporated hollow N-doped carbon spheres.

2.3. Structural Modifications of Doped Photocatalysts

The effects of metal doping on structural and morphological characteristics had been investigated via characterization of the doped and undoped samples using standard characterization techniques—namely, SEM, XRD, UV-Vis spectroscopy, FTIR and energy dispersive X-ray spectroscopy. In one of the studies on nickel-doped ZnO, the diffraction peaks obtained in the sample were sharper than in the undoped one, indicating the strong crystalline nature of the doped sample, which increased with dopant concentration and pH. However, the hexagonal wurtzite structure of the original undoped photocatalyst remained unchanged in the doped one [26]. However, an increase in dopant concentration beyond a critical concentration increased the agglomeration of the particles with a subsequent increase in the energy band gap, which was undesirable. Similarly, in pure TiO₂ and silver-doped TiO₂, the main phase was identified as anatase with no alteration in the crystal structure in the doped sample. The grain sizes calculated using the Debye-Scherrer formula were between 16–18 nm in undoped and doped samples, indicating the negligible impact of doping on grain sizes [32]. The Debye-Scherrer equation is given as

$$D = \frac{0.9\lambda}{\beta \cos \theta} \quad (1)$$

Here, D represents the grain size, λ is the wavelength of the Cu-K α line, β is the full width at half maxima (FWHM), and θ is the Bragg angle. Furthermore, the optical band gap energy was calculated using the Tauc equation as follows:

$$\alpha = K \frac{(h\nu - E_g)^2}{h\nu} \quad (2)$$

Here, K is a constant; $h\nu$ is the energy of the incident photon, e.g., the band gap energy for indirect transitions; and α is the absorption coefficient. It was observed that E_g decreased with the increasing concentration of silver, indicating a delay in the recombination of the electron–hole pair, resulting in improvement in photocatalytic activity. In another instance, a nickel- and zinc-doped barium hexaferrite photocatalyst was fabricated using the microemulsion route, and XRD analysis confirmed a hexagonal structure with zinc and nickel ions substituting barium and iron cations at the tetrahedral and octahedral positions. An increase in dopant concentration reduced the band gap energy, indicating a beneficial effect of doping on the photocatalytic activity. This was further confirmed by the decrease in intensity of the peak in the photoluminescence study [72]. The doped nanoparticle was porous, as indicated by a bulk density value as low as 0.13 kg/m³. Further co-doping with metal ions imparted exceptional stability to the catalysts, as demonstrated by the retention of photocatalytic efficiency after multiple cycles [34,72].

In a recent study, a one-pot synthesis of photocatalyst SrTiO₃, doubly modified with silver nanoparticles, was carried out to yield highly stable photocatalysts with BET surface areas as high as 16 m² g^{−1}, pore size of 19 nm, and a reduction in the energy band from 3.2 eV in undoped catalysts to 2.8 eV in the modified ones. The double modifications carried out were the following: doping the photocatalysts with silver nanoparticles and depositing the nanoparticles on the catalyst surface via wet impregnation method [73]. In the recent study on MXene-based TiO₂ catalysts, the specific surface area of hierarchical flower-like TiO₂ microspheres decorated with dual cocatalysts—namely, Ti₃C₂ nanosheets and Ag—measured using N₂ adsorption–desorption isotherms was ~100 m²/g, a value slightly lower than pristine TiO₂. However, the photocatalytic hydrogen production by the composite catalyst was 40-fold compared to the pristine TiO₂, indicating that the specific surface area did not play a significant role in enhancing the photocatalytic activity of the catalyst, although the adsorption of H₂O was an essential step in promoting photocatalytic hydrogen production [54].

XRD patterns of a sulphur-doped Sn₃O₄ photocatalyst indicated that the crystal structures of the catalyst remained unchanged due to doping. Narrowing the bandgap to 2.39–2.43 eV, a value smaller than that of pure Sn₃O₄, was achieved via sulphur doping. However, SEM studies indicated the destruction of the hierarchical flower-like structure of Sn₃O₄ due to sulphur doping [74].

3. The Doping of Adsorbents with Nanoparticles

Conventional adsorbents like activated carbon and alumina had been longstanding workhorses in removing dyes, heavy metals, and organic pollutants from wastewater [75]. However, the quest for more efficient and cost-effective wastewater treatment had shifted the focus towards low-cost adsorbents characterized by rapid adsorption kinetics and exceptional adsorptive capabilities [76]. Nanoadsorbents have emerged as promising alternatives to their conventional counterparts in this pursuit.

The superiority of nanoadsorbents lies in their distinct features, notably their remarkable surface area-to-volume ratio, customizable pore sizes, and reduced intraparticle diffusional distances. These characteristics translate into significantly enhanced performance when it comes to the adsorption of pollutants from wastewater. But the story does not end there; researchers had explored a novel approach to elevate the efficacy of nanoadsorbents even further—doping with external agents.

In this context, doping represents the infusion of specific compounds or elements into the nano-adsorbent matrix. This infusion process is not limited to a single method; it can

be achieved through chemical impregnation or mechanical mixing, offering flexibility in implementation. Heteroatom doping, a prominent technique, involves the substitution of surface carbon atoms with heteroatoms of varying sizes and electronegativities. This substitution brings about an intriguing phenomenon known as charge-transfer doping, wherein the charge distribution within the material was modulated, leading to altered adsorption behaviour. Alternatively, defective doping introduces structural imperfections or defects into the adsorbent's architecture, further influencing its adsorption characteristics.

Nitrogen stands out as a widely favoured choice among the array of elements employed as dopants. Nitrogen doping introduces unique properties to the adsorbent, effectively augmenting its pollutant removal capabilities [75]. In parallel, incorporating metal nanoparticles into adsorbents had also garnered significant attention. These metal nanoparticle-doped adsorbents offer distinct advantages [76], rendering them increasingly indispensable in wastewater treatment.

In essence, the adoption of nano adsorbents signifies a substantial leap in wastewater treatment technology. Their innate properties make them formidable candidates for pollutant removal. However, researchers can fine-tune these materials by leveraging the power of doping with external agents, enhancing their efficiency and versatility. Nitrogen and metal nanoparticle doping exemplify the innovative avenues explored to create advanced adsorbent materials tailored to meet the evolving demands of efficient pollutant removal from wastewater streams.

3.1. Nitrogen Doping

Removing carbon dioxide (CO₂) from flue gas using porous carbon adsorbents holds significant promise as a practical technique, primarily due to several advantageous factors. These include the ready availability of the adsorbent, its inherent selectivity towards CO₂, the simplicity of synthesis methods, and its robust stability even in harsh environmental conditions. The underlying principle of CO₂ adsorption onto carbon materials primarily relies on Van der Waals interactions, which facilitate the physical trapping of CO₂ molecules within a porous structure. However, researchers have harnessed the power of chemical doping to engineer the surface properties of porous carbon materials intentionally.

In this context, doping entails introducing specific impurities or atoms into the carbon lattice, effectively creating tailored electrostatic interactions during the adsorption process. This deliberate alteration induced by doping leads to variations in electron density across the carbon material, giving rise to micro-domains within the pore volume with distinct electrostatic strengths [77]. Among the elements considered for doping, nitrogen, boron, phosphorus, and sulphur—known for their relatively higher electronegativity—stand out. When incorporated into the carbon structure, these dopants introduce a positive charge density on neighbouring carbon atoms, enhancing oxygen molecules' adsorption affinity [78].

The strategic introduction of nitrogen atoms into the carbon framework, coupled with subsequent chemical activation, represents a particularly effective approach to maximize the number of active adsorption sites. Nitrogen, in particular, enjoys the status of a favoured dopant for carbon materials due to its closely matched atomic size with carbon and the possession of five valence electrons that readily facilitate bonding with carbon atoms.

Notably, nitrogen-doped carbon adsorbents can be synthesized through various methods, depending on whether the doping process occurs *in situ* or as a post-treatment step. *In situ*, nitrogen doping methods encompass solvothermal techniques, arc-discharge methods, substituting nitrogen atoms into the carbon structure during chemical vapor deposition from a nitrogen source, and nonmechanical approaches like ball milling. Conversely, post-treatment doping methods typically involve incorporating nitrogen atoms into available sites created by defects through annealing, hydrothermal treatments, ion implantation, or plasma treatments [78].

Overall, the utilization of porous carbon adsorbents for CO₂ removal from flue gas had garnered considerable attention due to their unique attributes. Nevertheless, by strategically introducing heteroatoms such as nitrogen into the carbon lattice through

doping, researchers can significantly enhance the adsorption properties, opening up new avenues for tailoring these materials to achieve even greater efficiency in capturing CO₂ from industrial emissions.

Synthesis of Nitrogen-Doped Adsorbent

The synthesis of nitrogen-doped adsorbents, particularly porous carbon materials, had attracted significant attention among researchers due to their exceptional adsorption capabilities. Various methodologies had been explored to create these adsorbents with tailored properties. In one study, two prepolymer solutions were prepared according to established protocols, one containing resorcinol and formaldehyde dissolved in water and another containing melamine and formaldehyde in water. These two precursor solutions were combined with graphene oxide, forming graphene oxide/melamine resin composites. Nitrogen-doped graphene oxide/melamine nanocomposites with abundant pores and a high surface area were synthesized through a hydrothermal reaction at 80 °C for 24 h to enhance their adsorption capacity further. The resulting composites were subjected to activation in a nitrogen stream, facilitated by a KOH activator, at temperatures ranging from 400 °C to 700 °C for 2 h. Subsequent washing and vacuum drying of the product post-pyrolysis resulted in the desired composite material [79].

In another study, nitrogen-doped porous carbon was prepared by mixing a nitrogen source, specifically carbamide, with anthracite coal particles, along with the activating agent KOH. This mixture was then heated to carbonization temperatures ranging around 800 °C for 4 h. After carbonization, the chips were carefully washed, dried overnight, and subsequently utilized for the adsorption of sulphur dioxide (SO₂) [80].

Innovative approaches had also been adopted in the synthesis of nitrogen-doped adsorbents. For instance, nitrogen-rich carbon precursor materials, such as renewable leather solid wastes, had been harnessed as a source of porous carbon material. These materials were employed to prepare KOH-activated nitrogen-doped adsorbents specifically designed for highly efficient removal of phenolic substances [81].

To provide a visual representation of the synthesis process, Figure 5 illustrates the schematic diagram depicting the synthesis of nitrogen-doped magnesium oxide-modified biochar-based adsorbent, exemplifying the innovative approaches undertaken in developing nitrogen-doped adsorbent materials [62]. These diverse methods collectively contribute to the advancement of adsorption technologies, offering promising solutions for various environmental and industrial applications.



Figure 5. Schematic diagram showing the synthesis of nitrogen-doped magnesium oxide modified biochar-based adsorbent (Copyright permission from [82]).

3.2. Metal Nanoparticle-Doped Adsorbents

Incorporating metal nanoparticles into adsorbents, known as metal doping, is a highly effective technique to enhance the separation efficiency and surface properties of the adsorbent materials. This process involves the deposition of metal nanoparticles onto the surface and within the pore channels of the adsorbent. Notably, metal doping introduces

active metal sites interacting with the carbon matrix, thereby improving the adsorbent's selectivity. Furthermore, doped metals' magnetic properties can facilitate the adsorbent's regeneration, making the process more efficient [83].

Metal nanoparticle doping had widespread application in wastewater treatment, extending beyond porous carbon materials to encompass various other porous adsorbents. Examples of these modified adsorbents include cellulose, zeolite, chitosan, and montmorillonite, each of which can be tailored for specific applications through metal doping. The mechanism underlying the doping of porous carbon material with metals is elucidated in Figure 6, which illustrates the interaction between metal and porous carbon [83].



Figure 6. The mechanism of doping between metal and porous carbon [83].

One particularly promising area of research involves the development of metal–organic framework (MOF)-based adsorbents doped with metal nanoparticles, such as nickel and copper. MOFs are crystalline porous materials characterized by metal centres interconnected by organic linkers. They offer substantial advantages, including high surface area, porosity, and exceptional thermal and chemical stability. Additionally, modifying the metal centres and linkers can customise MOFs' pore size and functionalities. Doping metal nanoparticles into MOFs can be achieved through various techniques, including chemical vapor deposition, solid grinding, microwave irradiation, and solution infiltration. Previous studies have demonstrated the effectiveness of MOF modification through palladium doping for toluene adsorption and cerium doping for NO₂ adsorption [84–86].

The incorporation of metals into metal oxide adsorbents can be accomplished using several strategies, such as chemical precipitation, sol–gel, solvothermal, and co-precipitation methods. For example, the solvothermal method had been employed to synthesize chromium-doped zinc oxide nanoparticles, efficiently removing methyl orange from wastewater [75]. Simultaneously, a hydrothermal approach was utilized to synthesize gadolinium-doped cobalt ferrite nanoparticles [68]. Additionally, the removal of radioactive iodine from an alkaline solution, a byproduct of nuclear fission in uranium, was effectively achieved using alumina doped with silver nanoparticles [87]. These diverse methods of metal nanoparticle doping continue to drive advancements in adsorption technologies, contributing to their efficacy in diverse environmental and industrial applications.

The Synthesis of Metal-Doped Adsorbents

In the synthesis of metal-doped adsorbents, various methods had been explored to effectively incorporate metal elements into the adsorbent matrix, enhancing their adsorption properties and suitability for specific applications. One study by Cheng et al. [88] employed ultrasound-assisted carbon activation as a key step. This process involved the activation of carbon, followed by impregnation with $\text{Fe}(\text{NO}_3)_3$ under an ultrasonic treatment for 30 min. Subsequent filtration and drying at 105 °C yielded the suspensions, which were then treated in a microwave to produce iron-doped activated carbon. During ultrasonic treatment, ultrasonic cavitation played a critical role, leading to an increase in the fixed carbon content and a corresponding decrease in other ingredients. This method resulted in the creation of iron-doped activated carbon with improved adsorption properties.

Another approach, the co-precipitation method, was employed to synthesize barium-doped zinc oxide nanoparticles, which exhibited high effectiveness as adsorbent materials for dyes [89]. This method involves the simultaneous precipitation of metal ions, resulting in the formation of doped nanoparticles with tailored properties suitable for dye removal applications.

Additionally, researchers had conducted a comparative study to evaluate the efficiencies of CO_2 adsorption using various metal-doped MgO adsorbents. This evaluation was based on theoretical calculations of adsorption energy, aiming to identify the most effective dopant for achieving maximum CO_2 removal [90]. Density Functional Theory (DFT) calculations played a crucial role in revealing that aluminium-doped MgO exhibited the highest average adsorption energy and the presence of chemisorption structures. Consequently, this interaction between CO_2 and aluminium-doped MgO was identified as the strongest and most favourable among the tested dopants. Due to their ease of separation, transition metals with magnetic properties—including nickel, iron, and cobalt—had been favoured as dopants. Nickel-carbon nanoparticles, for instance, were synthesised using an electrical wire explosion method under 320 V of voltage in an ethanol medium. Subsequent treatment processes, such as sonication, filtration, washing, and drying at 70 °C, yielded nano colloids that effectively removed organic dyes [91].

Furthermore, the modification of graphitic carbon nitride with various metals, including lithium, sodium, magnesium, and calcium, was explored. This involved annealing a mixture of cyanamide and the respective metal chloride at 550 °C for 3 h. The resulting synthesized material was assessed for its efficiency in dye removal applications [92]. These diverse methods of synthesizing metal-doped adsorbents showcase the versatility of approaches available for tailoring adsorption materials to meet specific environmental and industrial needs.

3.3. Recent Advancements in Doped Adsorbents

A number of investigations had been carried out recently for developing novel porous adsorbent material—namely, metal-organic frameworks, porous polymers, and engineered porous carbon with enhanced adsorption capacities and selectivity. Activated carbon cloth fabricated from precursors like viscous rayon, cotton, and blends and decorated with polypyrrole nanoparticles had been used extensively in CO_2 adsorption with a high $\text{CO}_2:\text{CH}_4$ selectivity. In a recent study, composites of viscose rayon cloth and polypyrrole nanoparticles (VRC-PNP) were prepared via polymerization followed by carbonization at 850 °C. Nickel doping was performed by immersing the composite fabric into a nickel solution, and the resulting composite achieved a $\text{CO}_2:\text{CH}_4$ selectivity of 369.5 at 20 bar and 298 K [93]. A facile one-pot synthesis of nitrogen-doped porous carbons was carried out by grinding a mixture of melamine, hexamethyltetramine, and pluronic; calcination was carried out in an N_2 atmosphere, and the mixture was used for drug adsorption with a capacity as high as 110 mg/g [94]. In another instance, nitrogen-doped hierarchical porous carbon was prepared by a step activation process with different proportions of cellulose, $(\text{NH}_4)_2\text{C}_2\text{O}_4$ and $\text{NaHCO}_3/\text{KHCO}_3$, and calcining at 900 °C. The nitrogen-doped hierarchical structure possessed a toluene adsorption capacity as high as 585 mg/g, where the micropores and the

nitrogen functional groups were the governing factors behind the nd toluene adsorption capacity [95].

The one-step urea hydrothermal method had been used to synthesise magnesium zirconium hydrotalcite-like material doped with Fe_2O_3 , and ZrO_2 , which were used for fluoride removal from water with an adsorption capacity as high as 113.38 mg/g. The metal oxide nanoparticles and the hexagonal laminae of the hydrotalcite were uniformly stacked, producing a large specific area of the adsorbent [96]. Recently, nitrogen-doped carboxylated porous carbon materials were employed to remove heavy metals from water—namely, lead, mercury, and chromium. In this work, four different nitrogen functional groups—namely, graphitic, pyrrolic, pyridinic and pyridine oxide—were combined with carboxyl acid functional groups and incorporated into the porous carbon structure, producing a BET surface area as high as 1135 m^2/g . A percentage removal of heavy metals as high as 100% was quickly achieved, which was attributed to its high adsorption capacity (721 mg/g for lead) and high uptake values [97]. The high specific surface area coupled with the chelating action of the carboxyl acid group synergistically increased the percentage removal of metal ions.

Recent studies had reported the synthesis of the nanocomposites of acid-functionalized carbon nanofibers with manganese-doped titanium nanotubes to recover lithium metal via adsorption. The functionalized carbon nanofibers (ACNF) were synthesized using hot mix acid oxidation, and the manganese-doped TNTs (Mn-TNT) were synthesized by a modified Murray approach. Microwave irradiation was used to deposit the Mn-TNTs on the ACNF. The lithium adsorption capacity of the nanocomposites was 10 times that of pristine ACNF [98]. Covalent triazine frameworks (CTF) were a recently developed promising class of adsorbents belonging to the triazine core covalent organic framework (COF) class. They were effectively employed for CO_2 capture [99] and dye removal from aqueous solutions [100]. A recent study employed a triazine-based covalent organic polymer with hierarchical micro and mesoporous structures to remove cationic and anionic dye, achieving a 50 mg/g adsorption capacity in an hour [100]. Phenylenediamine covalent organic polymer (PDA-COP) functionalized with 3-amino-1,2,4-triazole-5-thiol (ATT) was synthesized by a nucleophilic substitution reaction between cyanuric chloride and para-phenylenediamine, followed by a dropwise mixing of ATT. The ATT@PDA-COP showed a Hg^{2+} adsorption capacity of 312.5 mg/g [101]. A solvothermal method was used to synthesise a zinc-based coordination polymer adsorbent with a large surface area and porous structure to remove two dyes simultaneously using dimethyl formamide (DMF) and terephthalic acid (TP). The adsorption capacity of the prepared adsorbent for the two dyes—namely, quinoline and azure blue in the binary mixture—was 46.57 mg/g and 40.98 mg/g with a three time reusability without a decline in adsorption capacity [102]. Nitrogen-rich porous polymers obtained via co-polymerization of 1,4-bis-(2,4-diamino-1,3,5-triazine)-benzene with terephthaldehyde and with 1,3,5-tris(4-formylphenyl)benzene resulted in nitrogen-rich porous polymers with a surface area of 1579 m^2/g and 1028 m^2/g , respectively. The CO_2 uptake at 1 bar for the first adsorbent was 3.71 mmol/g at 298 K with a CO_2/N_2 selectivity of 21 and a CO_2/CH_4 selectivity of 5.3. The CO_2 uptake had been found to depend on pore functionality, while CH_4 uptake depended on surface area. Hence, the CO_2/CH_4 selectivity was found to be higher for the adsorbent with a lower surface area—namely, the second adsorbent [103].

4. Applications of Doped Photocatalysts and Adsorbents

Doping photocatalysts with metals and metal oxides enhances their photocatalytic properties, making them valuable in various applications. For instance, bismuth-doped TiO_2 had shown the synergistic enhancement of CO_2 photo-reduction and selectivity towards CH_4 [29]. Platinum had been used as an electron-trapping agent to modify bismuth-doped TiO_2 , effectively extracting trapped electrons on the surface of TiO_2 [8]. Other studies had explored the use of metal-doped photocatalysts for pollutant and dye removal, demonstrating their potential for environmental remediation [20,21]. Additionally,

metal oxides can serve as support materials for depositing catalysts, promoting catalytic activity, and improving overall performance [104].

Copper-doped zinc oxide had been employed for treating arsenic-rich water through the oxidation of arsenic (As(III) to As(V)) [105]. Researchers had also adopted unconventional strategies, like the solid-state method, to introduce iron into TiO₂ nanoparticles for preparing iron-doped TiO₂ photocatalysts for dye degradation [106]. Self-doping TiO₂ nanoparticles with Ti³⁺ had been achieved using a one-step solvothermal method, contributing to enhanced photocatalytic activity [107].

TiO₂ with manganese doping on reduced graphene oxide, synthesized through a one-pot hydrothermal method, exhibited a remarkable 99% chromium removal efficiency under sunlight within 60 min. Additionally, doping led to a significant 12.85% enhancement in photocatalytic activity [108].

Nanocomposites of TiO₂ and nitrogen-doped reduced graphene oxide were prepared via a urea-assisted hydrothermal method, showcased a noteworthy CO yield of 356.5 $\mu\text{mole g}^{-1}$ in CO₂ photoreduction reactions, representing a 4.4-fold increase compared to undoped TiO₂ [64].

Furthermore, nitrogen-doped graphene hydrogels were synthesized using a one-pot hydrothermal method, exhibited excellent adsorption and photocatalytic activities for organic pollutant removal. Doping led to a notable increase in the degradation percentage, from 60% to 70%, using the doped catalyst [109].

Fluorine-doped graphene nanosheet (FG)-based photocatalysts were modified with GdVO₄ via an ultrasonication-assisted hydrothermal method, achieved a remarkable 97% removal of phenol from water. Modification with GdVO₄ resulted in a substantial 120% enhancement in phenol degradation compared to pristine FG [67].

Self-doped reduced TiO₂ nanotube arrays (r-TiO₂ NTA), obtained through electrochemical self-doping, demonstrated a photocurrent density of 2.8 mA/cm² and a photoconversion efficiency of 1.27% in solar-assisted water-splitting reactions. This marked an increase from 0.97% in TiO₂ NTAs to 1.27% in electrochemically self-doped TiO₂ [110,111].

The list goes on to include Sn-doped haematite, platinum nanoparticle-doped mesoporous/ZnO photocatalysts, a magnetic NiFe₂O₄ catalyst supported on nitrogen-doped graphene, chitosan-based nitrogen-doped graphene, doped aluminium nanoparticles/*Moringa oleifera* gum-activated carbon, C-doped Bi₂O₃ nanowires, and neodymium (Nd³⁺)-doped CoFe₂O₄ (cobalt ferrite). These materials demonstrated significant improvements in their respective applications. The beneficial effects of doping photocatalysts through enhancement of their degradation efficiency are shown in Figure 7.

These diverse doping techniques and applications highlight the versatility of metal and metal oxide doping in tailoring the properties of photocatalytic materials, making them suitable for various environmental and catalytic applications.

Doping in adsorbents had played a pivotal role in augmenting their capabilities, leading to diverse applications. For example, a UiO-66 nanoparticle doped with cobalt and synthesized through a single-step solvothermal method, achieved a remarkable 94% removal of tetracycline, boasting 7.6 times greater adsorption capacity compared to pristine UiO-66 adsorbents [112].

In another instance, a bismuth oxide-doped MgO adsorbent, prepared via a co-precipitation method, demonstrated efficient indigo carmine dye adsorption with a maximum dye removal capacity of 126 mg g⁻¹, surpassing the performance of other magnesium-based adsorbents [113].

Additionally, Fe(NO₃)₃-impregnated activated carbon, synthesized using an ultrasound-microwave combined method, effectively removed dyes from wastewater, exhibiting a maximum adsorption capacity of 259.74 mg/g. The activation process improved the removal capacity by 17.12% compared to non-activated carbon [114].

Furthermore, nitrogen- and phosphorus-co-doped porous carbon, produced through a solvothermal method, displayed a remarkable CO₂ adsorption capacity of 5.68 mmol g⁻¹ at 5 bar, a 2.63-fold increase compared to the undoped adsorbent [115].

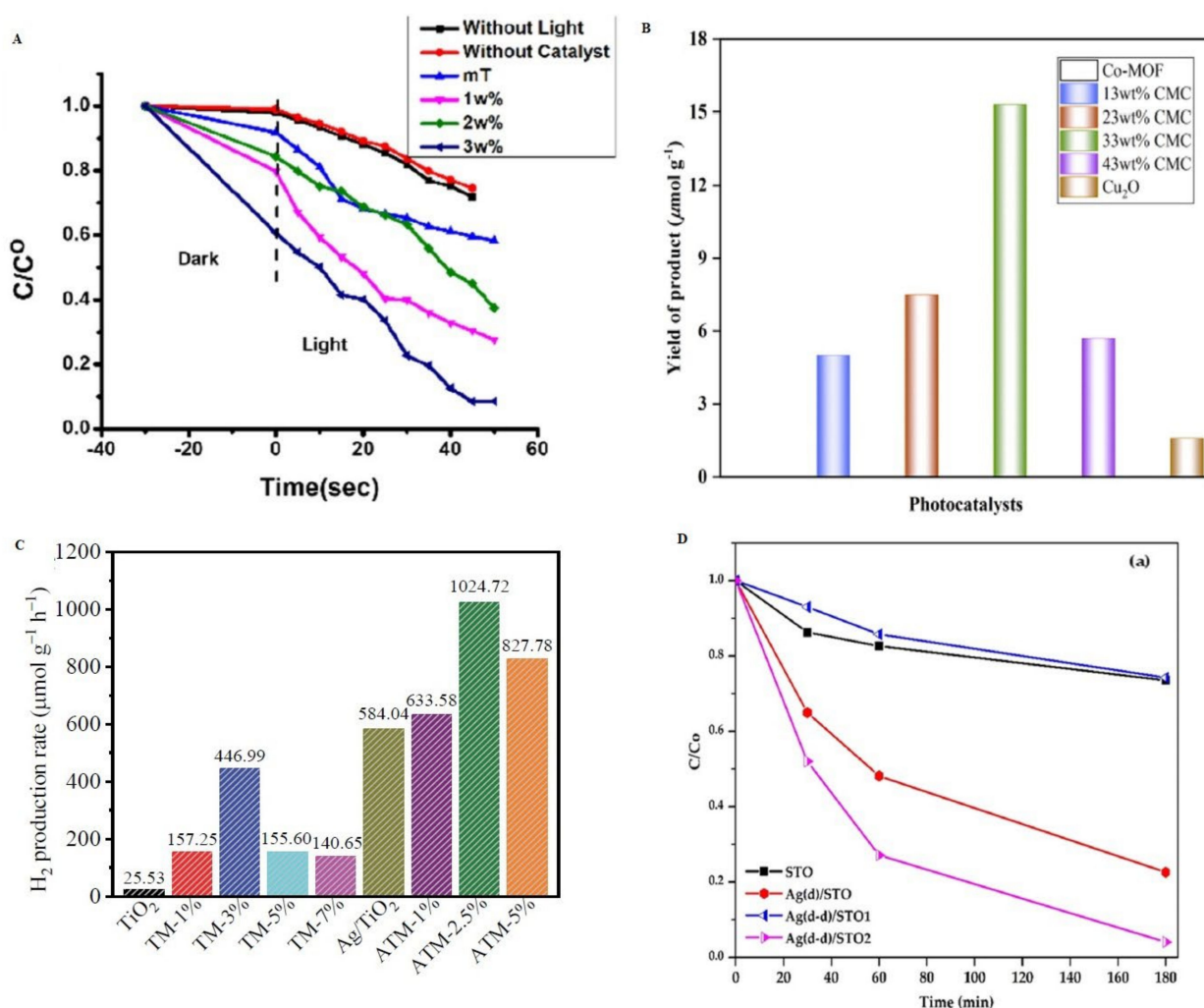


Figure 7. (A) Photocatalytic dye degradation comparison of undoped mesoporous TiO₂ (mT), 1wt% copper-doped mT, 2 wt% copper-doped mT, 3 wt and copper-doped mT, without light and without catalyst (Copyright permission from [34]). (B) Carbon monoxide evolution rate of a pure cobalt-based metal–organic framework (Co–MOF), Cu₂O and MOF/Cu₂O hybrid composites (CMC) composite samples with different weight percentages of Co–MOF during visible–light–driven CO₂ reduction (Copyright permission from [55]). (C) Photocatalytic hydrogen production of pure TiO₂, Ti₃C₂/TiO₂(TM) nanocomposites with different weight percentages of Ti₃C₂, Ag/TiO₂ composite, Ag/Ti₃C₂/TiO₂ nanocomposites with different weight percentages of Ag (Copyright permission from [54]). (D) Photocatalytic removal efficiency of NO_x with pure SrTiO₃ (STO), Ag–doped SrTiO₃ (Ag–STO), Ag-doped and Ag–deposited STO (Ag(d–d) STO1, Ag(d–d) STO2) where Ag in Ag (d–d) STO1 was obtained from Ag⁺ enriched solution, and Ag in Ag(d–d) STO2 was obtained from pure AgNO₃ solution. C₀ is the initial concentration and C the concentration after time t (reproduced from [73]).

Other examples include cerium oxide nanorods coated with nitrogen-doped carbon nanoparticles, nickel oxide nanoparticles, -doped PVA-MF polymer nanocomposites, zinc-doped SnS₂ nanoparticles, a metal–organic framework with the iron base loaded on iron oxide nanoparticles, nitrogen-doped biochar, and iron-doped natural clay. These materials showcased noteworthy enhancements in their adsorption capacities and efficiency for various applications [116–122]. The improvement of the performance of doped adsorbents over the undoped ones is demonstrated in Figure 8 for various applications.

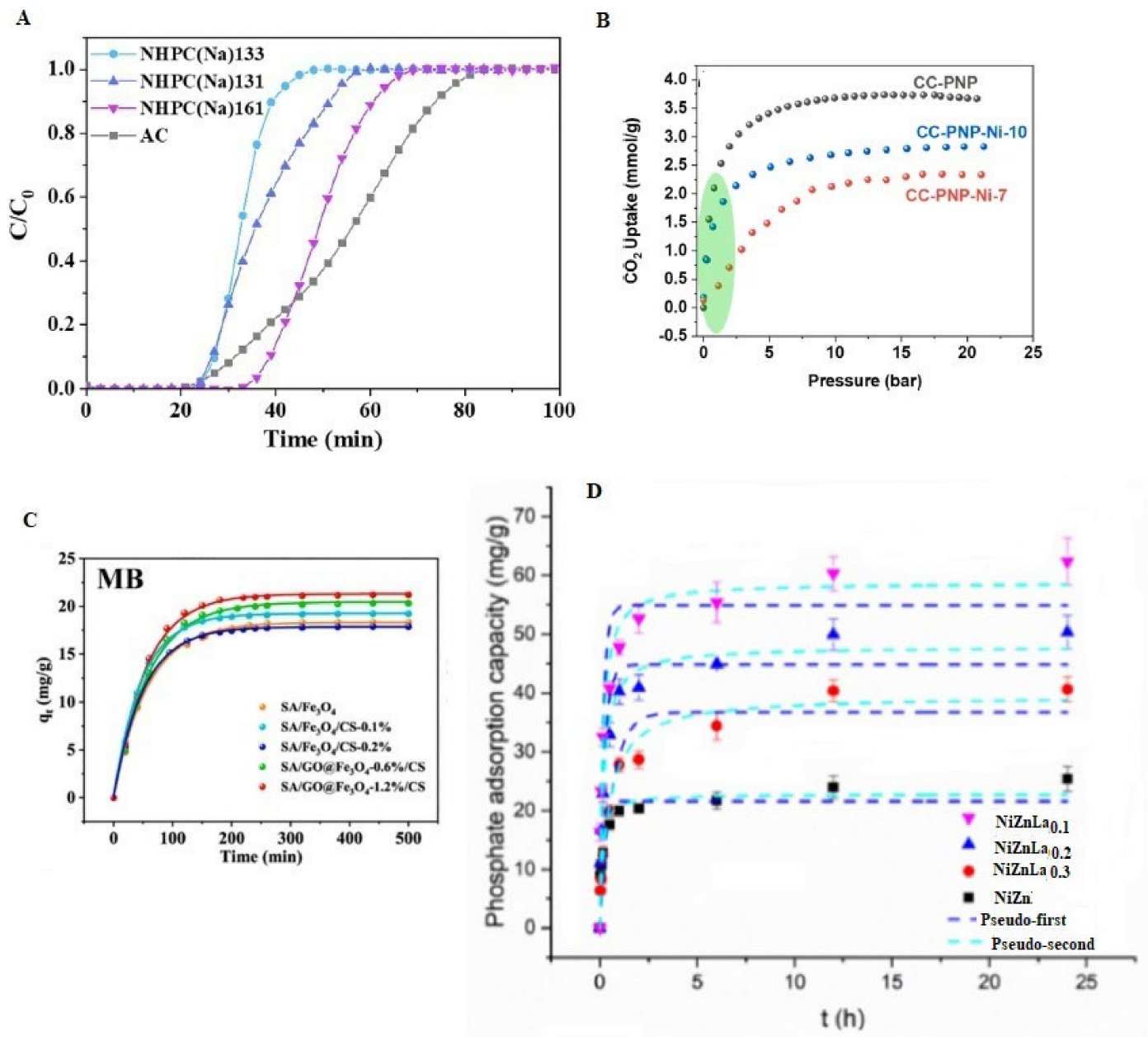


Figure 8. (A) Toluene adsorption breakthrough curves for nitrogen-doped hierarchical porous carbon (NHPC(Na)) prepared at different mass ratios of α -cellulose:(NH₄)₂C₂O₄:NaHCO₃ (133 indicates the mass ratio 1:3:3) and activated carbon (AC) (Copyright from [95]). (B) Adsorption isotherms of CO₂ uptake at different pressures using undoped carbonized viscose rayon-polyppyrrrole nanoparticles (CC-PNP) and nickel-doped CC-PNP with nickel content 7% (CC-PNP-Ni-7) and 10% (CC-PNP-Ni-10) (Copyright from [93]). (C) Adsorption kinetics of methylene blue removal by sodium alginate (SA), sodium alginate/Fe₃O₄ (SA/Fe₃O₄), sodium alginate/Fe₃O₄/chitosan (SA/Fe₃O₄/CS) at different weight percentages of chitosan (CS), graphene oxide (GO) modified Fe₃O₄-doped sodium alginate (SA)/chitosan (CS) gel at different percentages of CS (Copyright from [123]). (D) Phosphate adsorption kinetics of Lanthanum-doped trimetallic nickel zinc Lanthanum (NiZnLa) nanosheets and undoped nickel/zinc composites (Copyright from [124]).

To summarize, this section explores the broad spectrum of applications for metal and non-metal-doped photocatalysts and adsorbents, underscoring their significance in various environmental and industrial contexts. The findings from multiple studies are presented in Tables 1 and 2, offering comprehensive insights into synthesis methods, key outcomes, and

substantial performance enhancements realized through doping in these materials. Overall, the tables underscore the transformative impact of doping in photocatalysts and adsorbents, opening new avenues for addressing critical environmental and industrial challenges.

Table 1. Applications of Doped Photocatalysts.

Material	Method of Synthesis	Key Findings	Performance Improvement by Doping	References
Iron-based metal–organic framework (MOF) with azobenzene tetracarboxylic acid organic linkers	Facile hydrothermal method	CH ₄ product yield as high as 16.32 $\mu\text{mol g}^{-1}$ catalyst and 77.57% selectivity during visible light-driven CO ₂ photoreduction	Product yield improved fourfold compared to the metal cluster Fe ₃ (μ_3 -O)-(CH ₃ COO) ₆	[56]
Nanocomposites of TiO ₂ and nitrogen-doped reduced graphene oxide	Urea-assisted hydrothermal method	CO yield 356.5 $\mu\text{mol g}^{-1}$ in CO ₂ photoreduction reaction	4.4-fold enhancement in the yield of carbon monoxide compared to undoped TiO ₂	[64]
Fluorine-doped graphene nanosheets (FG)-based photocatalyst modified with GdVO ₄	Ultrasonication-assisted hydrothermal method (Exfoliation method)	97% removal of phenol from water	120% enhancement in phenol degradation using GdVO ₄ modified FG catalyst compared to pristine FG	[67]
TiO ₂ with manganese doping grown on reduced graphene oxide	One-pot hydrothermal method	99% chromium removal efficiency in 60 min under sunlight	12.85% enhancement in photocatalytic activity in the doped catalyst	[108]
Nitrogen-doped graphene hydrogels	Facile one plot hydrothermal method	Excellent adsorption and photocatalytic activities for organic pollutant removal	Increase in degradation percentage from 60 to 70 using doped catalyst	[109]
Self-doped reduced TiO ₂ nanotube array (r-TiO ₂ NTA)	Electrochemical self-doping	Photocurrent density achieved was 2.8 mA/cm ² at 1.23 V vs. reversible hydrogen electrode (RHE) and photoconversion efficiency 1.27% in solar-assisted water-splitting reactions.	Photoconversion efficiency increases from 0.97% in TiO ₂ NTAs to 1.27% in electrochemically self-doped TiO ₂ .	[110,111]
Pyrazolyl porphyrinic nickel-based MOF	Hydrothermal method	CH ₄ product yield as high as 101 $\mu\text{mol g}^{-1}$ catalyst and 62.73% CH ₄ selectivity during visible light driven CO ₂ photoreduction	Product yield increased threefold compared to other porphyrinic MOF	[125]
Sn-doped haematite	Solution combustion synthesis	5% Sn-doped haematite shows 100% photocatalytic activity in dye degradation	Photocatalytic activity was intact after three cycles compared to the pristine haematite	[126]
Platinum nanoparticle-doped mesoporous/ZnO photocatalyst	Sol–gel synthesis	Methanol yield of 668 $\mu\text{mol g}^{-1}$ during CO ₂ photoreduction	18.5-fold higher CH ₃ OH yield than pristine ZnO	[127]
Magnetic NiFe ₂ O ₄ catalyst supported on nitrogen-doped graphene	One-step hydrothermal method	100% Methylene blue degradation in 3 h	-	[128]
Chitosan-based nitrogen-doped graphene	Pyrolysis	90 μmol hydrogen generation in 180 min from a water/methanol mixture	Increase from 20 μmol in undoped photocatalyst to 90 μmol in doped photocatalyst	[129]
Doped aluminium nanoparticles/ <i>Moringa oleifera</i> gum-activated carbon	Sol–gel method	~95% removal of nitrate and phosphate under LED	Increase in removal efficiency from ~30% using undoped catalyst to 95% in doped catalyst	[130]

Table 1. Cont.

Material	Method of Synthesis	Key Findings	Performance Improvement by Doping	References
C-doped Bi ₂ O ₃ nanowires	Solvothermal method using bismuth-based adsorbent as a precursor	98.9% photocatalytic removal of bisphenol	Increase in photocatalytic activity from 30% degradation of the pollutant with commercial Bi ₂ O ₃ to 98.9% in doped catalyst.	[131]
Neodymium (Nd ³⁺)-doped CoFe ₂ O ₄ (cobalt ferrite)	Solvothermal treatment	94.7% dye degradation	Increase dye degradation percentage from 29.4% in undoped cobalt ferrite to 94.7% in doped catalyst.	[132]

Table 2. Applications of nanoparticle-doped adsorbents.

Material	Synthesis Method	Applications and Key Findings	Performance Improvement by Doping	References
Bismuth oxide-doped MgO adsorbent.	Co-precipitation method	Indigo carmine dye adsorption with a maximum dye removal capacity of 126 mg g ⁻¹ was shown by 5% Bi ₂ O ₃ doped MgO.	The adsorption capacity of the material was higher than other magnesium-based adsorbents.	[113]
Fe(NO ₃) ₃ -impregnated activated carbon	Ultrasound–microwave combined method	Dye removal from wastewater. Maximum adsorption capacity 259.74 mg/g	The removal capacity of iron-activated carbon was enhanced by 17.12% compared to carbon without activation	[114]
Nitrogen- and phosphorus-co-doped porous carbon.	Solvothermal method	The CO ₂ adsorption capacity of 5.68 mmol g ⁻¹ at 5 bar	Adsorption of CO ₂ increased 2.63 times compared to the undoped adsorbent	[115]
Cerium oxide nanorod nanocomposite coated with nitrogen-doped carbon nanoparticles	Hydrothermal method	Cadmium ion (Cd ²⁺) adsorption with 99.9% removal at 10 mg adsorbent dosage and pH 8 at 10 ppm Cd ²⁺ concentration	–	[116]
Nickel oxide nanoparticle-doped PVA MF polymer nanocomposites	Co-precipitation and condensation	Congo red dye adsorption, dye removal efficiency of 80% was achieved	Increased in dye adsorption capacity from ~45% in undoped composites to ~80% in doped composites	[117]
Zinc-doped SnS ₂ nanoparticles	Thermal decomposition method	Rhodamine B adsorption up to ~90%	Dye adsorption increased from ~30% in undoped nanoparticles to ~90% in doped adsorbent.	[118]
Metal–organic framework with iron base loaded on iron oxide nanoparticles	Solvothermal method	Methyl red dye removal with an adsorption capacity of 600 mg/g	-	[119]
Nitrogen-doped biochar	Solvent-free heating at 800 °C	CO ₂ adsorption with maximum adsorption capacity 250 mg g ⁻¹ at 1 bar and 273 K and selectivity 38.24	Adsorption capacity increased from 121 mg g ⁻¹ to 250 mg g ⁻¹	[120]
Iron-doped natural clay	Mixing pretreated clay with iron sulphate solution	Maximum recovery of 38 mg g ⁻¹ phosphate from urban wastewater	Increase in phosphate removal efficiency from 21 mg g ⁻¹ in undoped clay to 38 mg g ⁻¹ in doped clay	[121]

Table 2. Cont.

Material	Synthesis Method	Applications and Key Findings	Performance Improvement by Doping	References
Reduced graphene oxide/gadolinium-doped ZnFe ₂ O ₄ .	One pot Solvothermal method	Maximum levofloxacin adsorption capacity of 70%	Enhanced adsorption capacity from 30% in undoped to 70% in doped composites	[122]
UiO-66 nanoparticle doped with cobalt	Single-step solvothermal method	94% removal of tetracycline	7.6 times greater adsorption capacity compared to pristine UiO-66 adsorbents	[112]

5. Integrated Photocatalyst-Adsorbent Systems with Doping

The integration of adsorption and photocatalytic degradation processes represents a highly effective approach for removing contaminants, capitalizing on the advantages of both methods while achieving enhanced removal efficiencies. Various synthesis techniques, including sol–gel, microwave-assisted, and wet chemical impregnation, were employed to create these hybrid systems. Numerous studies are reported in the literature—exploring the potential of integrated adsorption–photocatalytic units incorporating doping elements [133,134].

For instance, using the sol–gel method, a significant improvement in phenol degradation was achieved by synthesising a fluorine-doped TiO₂ supported on an activated carbon adsorbent. Under visible light, this integrated system exhibited an impressive 61.2% degradation rate, whereas the undoped counterpart managed only a 13% degradation rate [134].

In another study, zirconium-doped TiO₂ nanoparticles immobilized on delaminated clay, prepared via the sol–gel route, demonstrated enhanced photocatalytic activity under solar radiation. The doped unit achieved approximately 90% removal of antipyrine in just 4 h—notably, the pollutant degradation reaction rate correlated with the irradiation intensity [135].

In a more recent investigation, the co-doping of titania nanoparticles coated on activated carbon with cerium and nitrogen was carried out to improve the degradation efficiency of sodium isobutyl xanthate under visible radiation. Employing the sol–gel route for doping, the doped adsorbent–photocatalyst system exhibited an impressive removal efficiency of 96.3% within 5 h, with a cerium dosage of 2%. By contrast, the undoped unit achieved a mere removal rate of approximately 9.8% within the same timeframe [136].

Furthermore, iodine-doped biochar demonstrated efficient adsorptive and visible-light-driven photocatalytic capabilities in removing organic pollutants in a study conducted by Wang and colleagues. The hydrothermal treatment of biochar with iodine resulted in the doped sample, which, when integrated for adsorption and photocatalysis, achieved a remarkable 100% removal of the pollutants [137].

Cerium–bismuth oxides/oxynitrides prepared via doping bismuth in ceria using a chemical precipitation technique served as bifunctional adsorbent/photocatalysts in the effective removal of toxic organophosphate by reactive adsorption followed by photocatalytic degradation. A near 100% removal of methyl paraxon was achieved during the reactive adsorption [138].

These examples underscore the immense potential of integrated photocatalyst-adsorbent systems with doping elements to address complex contamination challenges and provide a glimpse into the promising future of environmental remediation technologies.

6. Conclusions and Future Perspective

In conclusion, the quest for efficient photocatalytic materials hinges on the crucial stability and durability requirements during real-time operation. While certain materials like metal sulphides and chalcogenides initially exhibit high photocatalytic activity, they were prone to photocorrosion under irradiation. By contrast, titanium dioxide (TiO₂) stands out as a highly stable photocatalyst with significant catalytic prowess. Among the various

phases of TiO_2 , the anatase phase emerges as the most active, although it necessitates short-wavelength light, typically around 350 nm, to initiate its catalytic activity. Researchers had actively explored doping with both metals and non-metals to harness TiO_2 's potential in the visible region and reduce carrier recombination rates.

However, it is crucial to acknowledge that doped photocatalysts come with certain limitations. Metal doping, for instance, can result in unstable materials prone to corrosion, with the metal dopant leaching over time, leading to a decline in photocatalytic activity [139]. On the other hand, non-metal doping often demands stringent preparation conditions, and maintaining an optimal dopant loading is paramount; otherwise, it can significantly impair the photocatalyst's activity. In response to these challenges, researchers had increasingly turned to co-doping with metals and non-metals as a strategy to mitigate the limitations of single-element doping. Metal-organic frameworks have attracted attention as potential adsorption and photocatalyst candidates for degrading organic contaminants. However, they suffer from limitations like metal ions and ligands leaching into the solution. To improve the structural stability, photocatalytic, and adsorptive ability during real-time operations, doping with graphene oxide, silver, and activated carbon for preparing MOF-based composites had been carried out. However, most of the studies report the performance of these composites in synthetic wastewater. Rigorous studies need to be performed to test the stability of these composites in industrial wastewater to ascertain their suitability for working with real-time effluents [140].

Although many studies have reported the enhancement of photocatalytic activities of doped catalysts, more studies need to be reported on the physicochemical stability and reusability of the doped photocatalysts while handling large volumes of industrial effluents. Rigorous studies need to be carried out on the possible combination of doped photocatalyst-based pollutant removal with biological means and electrodynamic removal. The fundamental quantification of the doped photocatalysts' reactivity, toxicity, and fate must be reported [141].

In volatile organic compound (VOC) degradation, metal/metal co-dopants, such as silver and vanadium co-doping in TiO_2 nanoparticles, had served a dual role: ensuring uniform metal dispersion on the photocatalyst and creating oxygen vacancies. In the case of non-metal co-dopants, research had demonstrated that co-doping with carbon and nitrogen in TiO_2 can synergistically enhance VOC degradation without altering the catalyst's morphology [142]. However, it is important to note that co-doping may also present challenges, including the potential for enhanced electron-hole pair recombination and nanoparticle shielding effects. Therefore, comprehensive studies are needed to investigate the impact of doping on photocatalyst structure and stability, identify optimal process parameters for maximising doped photocatalyst efficacy while minimizing dopant leaching, and assess the performance and stability of doped catalysts in large-scale industrial systems, particularly in reactors with high-temperature conditions and agitator speeds.

In the field of adsorbents, doping carbon-based materials with nitrogen holds promise for enhancing adsorption capabilities and improving CO_2/N_2 selectivity. Nitrogen doping facilitates CO_2 uptake by enhancing the surface area and promoting interactions between acidic CO_2 molecules and basic nitrogen functionalities. Notably, co-doping with nitrogen and oxygen had yielded adsorbents with the highest CO_2 adsorption capacity. However, the highest CO_2/N_2 selectivity was achieved when the doped adsorbent featured abundant basic nitrogen functional groups, such as pyridinic and pyrrolic groups, regardless of the specific surface area. Hence, synthesising carbon-based adsorbents with optimized ultra microporous surface areas and essential basic heteroatoms was crucial to achieving high CO_2 uptake values and selectivity [143].

The overall adsorption efficiency of an adsorbent was governed by the various mass transfer resistances encountered during the operation, and an in-depth analysis of the effect of doping on the mass transfer resistance needs to be carried out. For instance, in the case of fixed-bed adsorbents, the modelling of transport equations depends upon the mass transfer mechanism from the adsorbate to the adsorbent phase. Both intraparticle and external film

resistances need to be considered. The relative significance of the two mass transfer resistances is governed by the Biot number (kL/D), where D is the internal diffusion coefficient, k is the external film coefficient, and L is the characteristic dimension. The Biot number ranges from 5–500 in fixed beds, indicating significant mass transfer resistance in the particles. It had been observed that micropore diffusion resistance predominates over macropore and film resistances [103]. However, a detailed study on the mass transfer effects affecting the performance of the doped adsorbents in different contacting devices needs to be carried out to establish the viability and suitability of the adsorbent in real-time operations.

Looking ahead, further advancements in the field of photocatalysts and adsorbents should focus on addressing these challenges and optimizing doping strategies to meet the growing demand for efficient and sustainable environmental remediation technologies. Extensive research in large-scale systems, industrial reactors, and real-world applications will be instrumental in realizing the full potential of doped materials in tackling environmental pollution and promoting a cleaner, healthier future.

Author Contributions: Concept and structuring of manuscript: P.S., R.K.A., G.D.V., S.V. and M.S.C. Manuscript preparation: P.S., P.B., G.M., J.G., B.M., D.T. and R.K.A. All authors have read and agreed to the published version of the manuscript.

Funding: This research received no external funding.

Institutional Review Board Statement: Not required.

Informed Consent Statement: Not applicable.

Data Availability Statement: Not applicable due to review work.

Acknowledgments: The authors want to thank Sarada Paul Roy for language corrections.

Conflicts of Interest: The authors declare no conflict of interest.

References

1. Lin, C.; Song, Y.; Cao, L.; Chen, S. Effective Photocatalysis of Functional Nanocomposites Based on Carbon and TiO₂ Nanoparticles. *Nanoscale* **2013**, *5*, 4986–4992. [[CrossRef](#)]
2. Jagadale, T.C.; Takale, S.P.; Sonawane, R.S.; Joshi, H.M.; Patil, S.I.; Kale, B.B.; Ogale, S.B. N-Doped TiO₂ Nanoparticle Based Visible Light Photocatalyst by Modified Peroxide Sol-Gel Method. *J. Phys. Chem. C* **2008**, *112*, 14595–14602. [[CrossRef](#)]
3. Guan, B.; Yu, J.; Guo, S.; Yu, S.; Han, S. Porous Nickel Doped Titanium Dioxide Nanoparticles with Improved Visible Light Photocatalytic Activity. *Nanoscale Adv.* **2020**, *2*, 1352–1357. [[CrossRef](#)]
4. Thambiliyagodage, C.; Mirihana, S. Photocatalytic Activity of Fe and Cu Co-Doped TiO₂ Nanoparticles under Visible Light. *J. Solgel Sci. Technol.* **2021**, *99*, 109–121. [[CrossRef](#)]
5. Negi, C.; Kandwal, P.; Rawat, J.; Sharma, M.; Sharma, H.; Dalapati, G.; Dwivedi, C. Carbon-Doped Titanium Dioxide Nanoparticles for Visible Light Driven Photocatalytic Activity. *Appl. Surf. Sci.* **2021**, *554*, 149553. [[CrossRef](#)]
6. El-sayed, M.E.A. Nano-adsorbents for Water and Wastewater Remediation. *Sci. Total Environ.* **2020**, *739*, 139903. [[CrossRef](#)]
7. Khajeh, M.; Laurent, S.; Dastafkan, K. Nano-adsorbents: Classification, Preparation, and Applications (with Emphasis on Aqueous Media). *Chem. Rev.* **2013**, *113*, 7728–7768. [[CrossRef](#)]
8. Chakhtouna, H.; Benzeid, H.; Zari, N.; El Kacem Qaiss, A.; Bouhfid, R. Recent Progress on Ag/TiO₂ Photocatalysts: Photocatalytic and Bactericidal Behaviors. *Environ. Sci. Pollut. Res.* **2021**, *28*, 44638–44666. [[CrossRef](#)]
9. Medhi, R.; Marquez, M.D.; Lee, T.R. Visible-Light-Active Doped Metal Oxide Nanoparticles: Review of Their Synthesis, Properties, and Applications. *ACS Appl. Nano Mater.* **2020**, *3*, 6156–6185. [[CrossRef](#)]
10. Melchionna, M.; Fornasiero, P. Updates on the Roadmap for Photocatalysis. *ACS Catal.* **2020**, *10*, 5493–5501. [[CrossRef](#)]
11. Karuppasamy, P.; Ramzan Nilofar Nisha, N.; Pugazhendhi, A.; Kandasamy, S.; Pitchaimuthu, S. An Investigation of Transition Metal Doped TiO₂ Photocatalysts for the Enhanced Photocatalytic Decoloration of Methylene Blue Dye under Visible Light Irradiation. *J. Environ. Chem. Eng.* **2021**, *9*, 105254. [[CrossRef](#)]
12. Kanakaraju, D.; anakKutiang, F.D.; Lim, Y.C.; Goh, P.S. Recent Progress of Ag/TiO₂ Photocatalyst for Wastewater Treatment: Doping, Co-Doping, and Green Materials Functionalization. *Appl. Mater. Today* **2022**, *27*, 101500.
13. Akpan, U.G.; Hameed, B.H. The Advancements in Sol-Gel Method of Doped-TiO₂ Photocatalysts. *Appl. Catal. A Gen.* **2010**, *375*, 1–11. [[CrossRef](#)]
14. Bokov, D.; Turki Jalil, A.; Chupradit, S.; Suksatan, W.; Javed Ansari, M.; Shewael, I.H.; Valiev, G.H.; Kianfar, E. Nanomaterial by Sol-Gel Method: Synthesis and Application. *Adv. Mater. Sci. Eng.* **2021**, *2021*, 5102014. [[CrossRef](#)]
15. Miditana, S.R.; Tirukkovalluri, S.R.; Raju, I.M.; Babu, A.B.; Babu, A.R. Review on the Synthesis of Doped TiO₂ Nanomaterials by Sol-Gel Method and Description of Experimental Techniques. *J. Water Environ. Nanotechnol.* **2022**, *7*, 218–229.

16. Thomas, J.; Radhika, S.; Yoon, M. Nd³⁺-Doped TiO₂ Nanoparticles Incorporated with Heteropoly Phosphotungstic Acid: A Novel Solar Photocatalyst for Degradation of 4-Chlorophenol in Water. *J. Mol. Catal. A Chem.* **2015**, *411*, 146–156. [[CrossRef](#)]
17. Sun, D.; Wang, K.; Xu, Z.; Li, R. Synthesis and Photocatalytic Activity of Sulfate Modified Nd-Doped TiO₂ under Visible Light Irradiation. *J. Rare Earths* **2015**, *33*, 491–497. [[CrossRef](#)]
18. Lal, M.; Sharma, P.; Ram, C. Synthesis and Photocatalytic Potential of Nd-Doped TiO₂ under UV and Solar Light Irradiation Using a Sol-Gel Ultrasonication Method. *Results Mater.* **2022**, *15*, 100308. [[CrossRef](#)]
19. Nithya, N.; Bhoopathi, G.; Magesh, G.; Kumar, C.D.N. Neodymium Doped TiO₂ Nanoparticles by Sol-Gel Method for Antibacterial and Photocatalytic Activity. *Mater. Sci. Semicond. Process.* **2018**, *83*, 70–82. [[CrossRef](#)]
20. Avram, D.; Patrascu, A.A.; Istrate, M.C.; Cojocaru, B.; Tiseanu, C. Lanthanide Doped TiO₂: Coexistence of Discrete and Continuous Dopant Distribution in Anatase Phase. *J. Alloys Compd.* **2021**, *851*, 156849. [[CrossRef](#)]
21. Caschera, D.; Federici, F.; de Caro, T.; Cortese, B.; Calandra, P.; Mezzi, A.; Lo Nigro, R.; Toro, R.G. Fabrication of Eu-TiO₂ NCs Functionalized Cotton Textile as a Multifunctional Photocatalyst for Dye Pollutants Degradation. *Appl. Surf. Sci.* **2018**, *427*, 81–91. [[CrossRef](#)]
22. Luo, Y.; Wang, K.; Qian, Q.; Zheng, W.; Xue, H.; Huang, B.; Xiao, L.; Chen, Q. Fabrication and Photocatalytic Properties of Gd-Doped ZnO Nanoparticle-Assembled Nanorods. *Mater. Lett.* **2015**, *149*, 70–73. [[CrossRef](#)]
23. Mehtab, A.; Ahmed, J.; Alshehri, S.M.; Mao, Y.; Ahmad, T. Rare Earth Doped Metal Oxide Nanoparticles for Photocatalysis: A Perspective. *Nanotechnology* **2022**, *33*, 142001. [[CrossRef](#)] [[PubMed](#)]
24. Dhandapani, C.; Narayanasamy, R.; Karthick, S.N.; Hemalatha, K.V.; Selvam, S.; Hemalatha, P.; Kumar, M.S.; Kirupha, S.D.; Kim, H.J. Drastic Photocatalytic Degradation of Methylene Blue Dye by Neodymium Doped Zirconium Oxide as Photocatalyst under Visible Light Irradiation. *Optik* **2016**, *127*, 10288–10296. [[CrossRef](#)]
25. Zhang, J.; Deng, S.J.; Liu, S.Y.; Chen, J.M.; Han, B.Q.; Wang, Y.; Wang, Y.D. Preparation and Photocatalytic Activity of Nd Doped ZnO Nanoparticles. *Mater. Technol.* **2014**, *29*, 262–268. [[CrossRef](#)]
26. Zaman, Y.; Ishaque, M.Z.; Waris, K.; Shahzad, M.; Siddique, A.B.; Arshad, M.I.; Zaman, H.; Ali, H.M.; Kanwal, F.; Aslam, M.; et al. Modified Physical Properties of Ni Doped ZnO NPs as Potential Photocatalyst and Antibacterial Agents. *Arab. J. Chem.* **2023**, *16*, 105230. [[CrossRef](#)]
27. Choudhary, K.; Saini, R.; Purohit, L.P. Controllable Synthesis of Ce-Doped ZnO: TiO₂ Nanospheres for Photocatalytic Degradation of MB Dye and Levofloxacin under Sunlight Light Irradiation. *Opt. Mater.* **2023**, *143*, 114167. [[CrossRef](#)]
28. Palai, A.; Panda, N.R.; Sahu, D. Exploring the Photoluminescence Property, Photocatalytic Efficiency, and Antibacterial Activity of Eu-Doped ZnO/SnO₂ Heterostructure. *ECS J. Solid State Sci. Technol.* **2023**, *12*, 076015. [[CrossRef](#)]
29. Moradi, M.; Khorasheh, F.; Larimi, A. Pt Nanoparticles Decorated Bi-Doped TiO₂ as an Efficient Photocatalyst for CO₂ Photo-Reduction into CH₄. *Sol. Energy* **2020**, *211*, 100–110. [[CrossRef](#)]
30. Ochoa Rodríguez, P.A.; Pecchi, G.A.; Casuscelli, S.G.; Elías, V.R.; Eimer, G.A. A Simple Synthesis Way to Obtain Iron-Doped TiO₂ Nanoparticles as Photocatalytic Surfaces. *Chem. Phys. Lett.* **2019**, *732*, 136643. [[CrossRef](#)]
31. Sultana, R.; Liba, S.I.; Rahman, M.A.; Yeachin, N.; Syed, I.M.; Bhuiyan, M.A. Enhanced Photocatalytic Activity in RhB Dye Degradation by Mn and B Co-Doped Mixed Phase TiO₂ Photocatalyst under Visible Light Irradiation. *Surf. Interfaces* **2023**, *42*, 103302. [[CrossRef](#)]
32. Abbad, S.; Guergouri, K.; Gzaout, S.; Djebabra, S.; Zertal, A.; Barille, R.; Zaabat, M. Effect of Silver Doping on the Photocatalytic Activity of TiO₂ Nanopowders Synthesized by the Sol-Gel Route. *J. Environ. Chem. Eng.* **2020**, *8*, 103718. [[CrossRef](#)]
33. Pérez-González, M.; Tomás, S.A.; Santoyo-Salazar, J.; Gallardo-Hernández, S.; Tellez-Cruz, M.M.; Solorza-Feria, O. Sol-Gel Synthesis of Ag-Loaded TiO₂-ZnO Thin Films with Enhanced Photocatalytic Activity. *J. Alloys Compd.* **2019**, *779*, 908–917. [[CrossRef](#)]
34. Bibi, S.; Shah, S.S.; Muhammad, F.; Siddiq, M.; Kiran, L.; Aldossari, S.A.; Sheikh Saleh Mushab, M.; Sarwar, S. Cu-Doped Mesoporous TiO₂ Photocatalyst for Efficient Degradation of Organic Dye via Visible Light Photocatalysis. *Chemosphere* **2023**, *339*, 139583. [[CrossRef](#)] [[PubMed](#)]
35. Padmaja, B.; Dhanapandian, S.; Ashokkumar, K. Hydrothermally Derived Mg Doped Tin Oxide Nanostructures for Photocatalytic and Supercapacitor Applications. *Mater. Sci. Eng. B* **2023**, *297*, 116699. [[CrossRef](#)]
36. Lertthanaphol, N.; Pienutsa, N.; Chusri, K.; Sornsuchat, T.; Chanthara, P.; Seeharaj, P.; Kim-Lohsoontorn, P.; Srinives, S. One-Step Hydrothermal Synthesis of Precious Metal-Doped Titanium Dioxide–Graphene Oxide Composites for Photocatalytic Conversion of CO₂ to Ethanol. *ACS Omega* **2021**, *6*, 35769–35779. [[CrossRef](#)]
37. Sunkhunthod, C.; Jiamprasertboon, A.; Waehayee, A.; Untarabut, P.; Phonsuksawang, P.; Butburee, T.; Suthirakun, S.; Siritanon, T. Enhanced Tetracycline Photocatalytic Degradation of FeOx/Fe-Bi₂O₂CO₃ Synthesized by One-Step Hydrothermal Method. *J. Alloys Compd.* **2023**, *960*, 170632. [[CrossRef](#)]
38. Tarasenko, N.; Kornev, V.; Ramanenka, A.; Li, R.; Tarasenko, N. Photoluminescent Neodymium-Doped ZnO Nanocrystals Prepared by Laser Ablation in Solution for NIR-II Fluorescence Bioimaging. *Heliyon* **2022**, *8*, e09554. [[CrossRef](#)]
39. Chemin, A.; Lam, J.; Laurens, G.; Trichard, F.; Motto-Ros, V.; Ledoux, G.; Jarý, V.; Laguta, V.; Nikl, M.; Dujardin, C.; et al. Doping Nanoparticles Using Pulsed Laser Ablation in a Liquid Containing the Doping Agent. *Nanoscale Adv.* **2019**, *1*, 3963–3972. [[CrossRef](#)]
40. Siritwong, C.; Wetchakun, N.; Inceesungvorn, B.; Channei, D.; Samerjai, T.; Phanichphant, S. Doped-Metal Oxide Nanoparticles for Use as Photocatalysts. *Prog. Cryst. Growth Charact. Mater.* **2012**, *58*, 145–163. [[CrossRef](#)]

41. Psathas, P.; Zindrou, A.; Papachristodoulou, C.; Boukos, N.; Deligiannakis, Y. In Tandem Control of La-Doping and CuO-Heterojunction on SrTiO₃ Perovskite by Double-Nozzle Flame Spray Pyrolysis: Selective H₂ vs. CH₄ Photocatalytic Production from H₂O/CH₃OH. *Nanomaterials* **2023**, *13*, 482. [[CrossRef](#)]
42. Trung Tran, S.B.; Choi, H.S.; Oh, S.Y.; Moon, S.Y.; Park, J.Y. Iron-Doped ZnO as a Support for Pt-Based Catalysts to Improve Activity and Stability: Enhancement of Metal-Support Interaction by the Doping Effect. *RSC Adv.* **2018**, *8*, 21528–21533. [[CrossRef](#)] [[PubMed](#)]
43. Radha, B.; Rathi, R.; Lalithambika, K.C.; Thayumanavan, A.; Ravichandran, K.; Sriram, S. Effect of Fe Doping on the Photocatalytic Activity of ZnO Nanoparticles: Experimental and Theoretical Investigations. *J. Mater. Sci. Mater. Electron.* **2018**, *29*, 13474–13482. [[CrossRef](#)]
44. Rani, M.; Keshu; Pandey, S.; Rishabh; Sharma, S.; Shanker, U. Sunlight Assisted Highly Efficient Photocatalytic Remediation of Organic Pollutants by Green Biosynthesized ZnO@WO₃ Nanocomposite. *J. Photochem. Photobiol. A Chem.* **2024**, *446*, 115160. [[CrossRef](#)]
45. Zeid, E.F.F.A.; Obiedallah, F.M.M.; Abu-Sehly, A.H.; Mohamed, W.A.A.; El-Aal, M.A. A Comparative Study of Single and Bi-Doped Co₃O₄ Nanocatalysts for the Photodegradation of Methyl Orange Dye. *J. Mol. Struct.* **2023**, *1293*, 136203. [[CrossRef](#)]
46. Ahmadi, N.; Nemati, A.; Bagherzadeh, M. Synthesis and Properties of Ce-Doped TiO₂-Reduced Graphene Oxide Nanocomposite. *J. Alloys Compd.* **2018**, *742*, 986–995. [[CrossRef](#)]
47. Velázquez-Martínez, S.; Silva-Martínez, S.; Pineda-Arellano, C.A.; Jiménez-González, A.; Salgado-Tránsito, I.; Morales-Pérez, A.A.; Peña-Cruz, M.I. Modified Sol-Gel/Hydrothermal Method for the Synthesis of Microsized TiO₂ and Iron-Doped TiO₂, Its Characterization and Solar Photocatalytic Activity for an Azo Dye Degradation. *J. Photochem. Photobiol. A Chem.* **2018**, *359*, 93–101. [[CrossRef](#)]
48. Baig, F.; Butt, G.S. Impact of Copper Doping on Optical, UV Induced Wettability and Photo-Catalytic Properties of Sol-Gel Synthesized ZnO Thin Films. *Optik* **2023**, *288*, 171196. [[CrossRef](#)]
49. Hameeda, B.; Mushtaq, A.; Saeed, M.; Munir, A.; Jabeen, U.; Waseem, A. Development of Cu-Doped NiO Nanoscale Material as Efficient Photocatalyst for Visible Light Dye Degradation. *Toxin Rev.* **2021**, *40*, 1396–1406. [[CrossRef](#)]
50. Soleimani-Gorgani, A.; Al-Hazmi, H.E.; Esmaeili, A.; Habibzadeh, S. Screen-Printed Sn-Doped TiO₂ Nanoparticles for Photocatalytic Dye Removal from Wastewater: A Technological Perspective. *Environ. Res.* **2023**, *237*, 117079. [[CrossRef](#)]
51. Vishnu, G.; Singh, S.; Kaul, N.; Ramamurthy, P.C.; Naik, T.S.S.K.; Viswanath, R.; Kumar, V.; Bhojya Naik, H.S.; Prathap, A.; Anil Kumara, H.A.; et al. Green Synthesis of Nickel-Doped Magnesium Ferrite Nanoparticles via Combustion for Facile Microwave-Assisted Optical and Photocatalytic Applications. *Environ. Res.* **2023**, *235*, 116598. [[CrossRef](#)]
52. Azimi-Fouladi, A.; Falak, P.; Hassanzadeh-Tabrizi, S.A. The Photodegradation of Antibiotics on Nano Cubic Spinel Ferrites Photocatalytic Systems: A Review. *J. Alloys Compd.* **2023**, *961*, 171075.
53. Naik, M.M.; Naik, H.S.B.; Nagaraju, G.; Vinuth, M.; Vinu, K.; Rashmi, S.K. Effect of Aluminium Doping on Structural, Optical, Photocatalytic and Antibacterial Activity on Nickel Ferrite Nanoparticles by Sol-Gel Auto-Combustion Method. *J. Mater. Sci. Mater. Electron.* **2018**, *29*, 20395–20414. [[CrossRef](#)]
54. Liu, D.; Sun, B.; Bai, S.; Gao, T.; Zhou, G. Dual Co-Catalysts Ag/Ti₃C₂/TiO₂ Hierarchical Flower-like Microspheres with Enhanced Photocatalytic H₂-Production Activity. *Chin. J. Catal.* **2023**, *50*, 273–283. [[CrossRef](#)]
55. Dong, W.W.; Jia, J.; Wang, Y.; An, J.R.; Yang, O.Y.; Gao, X.J.; Liu, Y.L.; Zhao, J.; Li, D.S. Visible-Light-Driven Solvent-Free Photocatalytic CO₂ Reduction to CO by Co-MOF/Cu₂O Heterojunction with Superior Selectivity. *Chem. Eng. J.* **2022**, *438*, 135622. [[CrossRef](#)]
56. An, J.R.; Wang, Y.; Dong, W.W.; Gao, X.J.; Yang, O.Y.; Liu, Y.L.; Zhao, J.; Li, D.S. Efficient Visible-Light Photoreduction of CO₂ to CH₄ over an Fe-Based Metal-Organic Framework (PCN-250-Fe₃) in a Solid-Gas Mode. *ACS Appl. Energy Mater.* **2022**, *5*, 2384–2390. [[CrossRef](#)]
57. Yang, O.Y.; Gao, X.J.; Qi, G.D.; Wang, Y.; Dong, W.W.; Tian, Z.F.; Zhao, J.; Li, D.S.; Zhang, Q. Dye-Anchoring Strategy with a Metal-Organic Framework for a Highly Efficient Visible-Light-Driven Photocatalytic CO₂ Reduction through the Solid-Gas Mode. *ACS Appl. Energy Mater.* **2023**, *6*, 334–341. [[CrossRef](#)]
58. Wang, W.; Sheng, Q.; Zhi, G.; Zhao, Y.; Qu, R.; Sun, L.; Zhang, S. A Strategy of Adjusting Band Alignment to Improve Photocatalytic Degradation and Photocatalytic Hydrogen Evolution of CuSbS₂. *Appl. Surf. Sci.* **2023**, *639*, 158251. [[CrossRef](#)]
59. Teng, Z.; Wang, B.; Hu, Y.; Zhang, W.; Wu, Z.; Xu, D. High Performance Ultrafiltration Membrane by Coupling Magnetic Migration and In-Situ Surface Modification. *Polym. Test.* **2021**, *101*, 107306. [[CrossRef](#)]
60. Wang, L.; Sun, M.; Zhu, S.; Zhang, M.; Ma, Y.; Xie, D.; Li, S.; Mominou, N.; Jing, C. Cu-Ni Bimetallic Single Atoms Supported on TiO₂@NG Core-Shell Material for the Removal of Dibenzothiophene under Visible Light. *Sep. Purif. Technol.* **2021**, *279*, 119646. [[CrossRef](#)]
61. Zhang, Z.-R.; Guo, R.-T.; Xia, C.; Li, C.-F.; Pan, W.-G. B-TiO₂/CuInS₂ Photocatalyst Based on the Synergistic Effect of Oxygen Vacancy and Z-Scheme Heterojunction for Improving Photocatalyst CO₂ Reduction. *Sep. Purif. Technol.* **2023**, *323*, 124461. [[CrossRef](#)]
62. Liu, S.H.; Syu, H.R. High Visible-Light Photocatalytic Hydrogen Evolution of C,N-Codoped Mesoporous TiO₂ Nanoparticles Prepared via an Ionic-Liquidtemplate Approach. *Int. J. Hydrogen Energy* **2013**, *38*, 13856–13865. [[CrossRef](#)]
63. Ansari, S.A.; Khan, M.M.; Ansari, M.O.; Cho, M.H. Nitrogen-Doped Titanium Dioxide (N-Doped TiO₂) for Visible Light Photocatalysis. *New J. Chem.* **2016**, *40*, 3000–3009. [[CrossRef](#)]

64. Lin, L.-Y.; Nie, Y.; Kavadiya, S.; Soundappan, T.; Biswas, P. N-Doped Reduced Graphene Oxide Promoted Nano TiO₂ as a Bifunctional Adsorbent/Photocatalyst for CO₂ Photoreduction: Effect of N Species. *Chem. Eng. J.* **2017**, *316*, 449–460. [CrossRef]
65. Mersal, M.; Zedan, A.F.; Mohamed, G.G.; Hassan, G.K. Fabrication of Nitrogen Doped TiO₂/Fe₂O₃ Nanostructures for Photocatalytic Oxidation of Methanol Based Wastewater. *Sci. Rep.* **2023**, *13*, 4431. [CrossRef]
66. Ellouzi, I.; El Hajjaji, S.; Harir, M.; Schmitt Koplín, P.; Robert, D.; Laânab, L. Synergistic Effects of C, N, S, Fe-Multidoped TiO₂ for Photocatalytic Degradation of Methyl Orange Dye under UV and Visible Light Irradiations. *SN Appl. Sci.* **2019**, *1*, 930. [CrossRef]
67. Shandilya, P.; Mittal, D.; Sudhaik, A.; Soni, M.; Raizada, P.; Saini, A.K.; Singh, P. GdVO₄ Modified Fluorine Doped Graphene Nanosheets as Dispersed Photocatalyst for Mitigation of Phenolic Compounds in Aqueous Environment and Bacterial Disinfection. *Sep. Purif. Technol.* **2019**, *210*, 804–816. [CrossRef]
68. Toe, E.D.; Kurniawan, W.; Mariquit, E.G.; Hinode, H. Synthesis of N-Doped Mesoporous TiO₂ by Facile One-Step Solvothermal Process for Visible Light Photocatalytic Degradation of Organic Pollutant. *J. Environ. Chem. Eng.* **2018**, *6*, 5125–5134. [CrossRef]
69. Tao, F.T.; Hu, C.; Wu, J.C.S.; Nguyen, V.H.; Tung, K.L. Influence of Nitrogen Sources on N-Doped Reduced TiO₂ Prepared Using Atmospheric Plasma Spraying for Photocatalytic Tetracycline and Ciprofloxacin Degradation. *Sep. Purif. Technol.* **2023**, *326*, 124784. [CrossRef]
70. Guan, J.; Li, D.; Feng, J.; Xu, P.; Li, Z.; Ge, S.; Chen, H.; Zhang, K. Enhanced Photocatalytic Ammonia Oxidation Activity and Nitrogen Selectivity over Ag/AgCl/N-TiO₂ Photocatalyst. *J. Environ. Sci.* **2024**, *138*, 395–405. [CrossRef]
71. Liu, X.; Wang, J.; Liao, T.; Li, Y.; Fan, X.; Zhang, F.; Peng, W. Electron Transfer Route Tuning Caused by Photo-Irradiation: Stability Enhancement of N-Doped Carbon Materials in Fenton-like Reactions. *Appl. Catal. B* **2024**, *340*, 123261. [CrossRef]
72. Mustafa, G.; Bibi, I.; Majid, F.; Sultan, M.; Taj, B.; Nazeer, Z.; Muhammad Umair, H.; Elqahtani, Z.M.; Alwadai, N.; Khan, M.I.; et al. Zn and Ni Doping Effect on Barium Hexaferrite Ferroelectric, Optical Properties and Photocatalytic Activity under Visible Light Irradiation. *Phys. B Condens. Matter* **2023**, *663*, 415006. [CrossRef]
73. Ordoñez, M.F.; Cerrato, G.; Giordana, A.; Di Michele, A.; Falletta, E.; Bianchi, C.L. One-Pot Synthesis of Ag-Modified SrTiO₃: Synergistic Effect of Decoration and Doping for Highly Efficient Photocatalytic NO_x Degradation under LED. *J. Environ. Chem. Eng.* **2023**, *11*, 110368. [CrossRef]
74. Zhang, L.; Liu, X.; Zhang, X.; Zhang, W.; Ma, J.; Wang, Q.; Su, S. Sulfur-Doped Sn₃O₄ Nanosheets for Improved Photocatalytic Performance. *J. Alloys Compd.* **2023**, *961*, 170904. [CrossRef]
75. Meng, A.; Xing, J.; Li, Z.; Li, Q. Cr-Doped ZnO Nanoparticles: Synthesis, Characterization, Adsorption Property, and Recyclability. *ACS Appl. Mater. Interfaces* **2015**, *7*, 27449–27457. [CrossRef]
76. Kumar, U.; Hassan, J.Z.; Bhatti, R.A.; Raza, A.; Nazir, G.; Nabgan, W.; Ikram, M. Photocatalysis vs Adsorption by Metal Oxide Nanoparticles. *J. Mater. Sci. Technol.* **2022**, *131*, 122–166. [CrossRef]
77. Kumar, K.V.; Preuss, K.; Lu, L.; Guo, Z.X.; Titirici, M.M. Effect of Nitrogen Doping on the CO₂ Adsorption Behavior in Nanoporous Carbon Structures: A Molecular Simulation Study. *J. Phys. Chem. C* **2015**, *119*, 22310–22321. [CrossRef]
78. Al-Hajri, W.; De Luna, Y.; Bensalah, N. Review on Recent Applications of Nitrogen-Doped Carbon Materials in CO₂ Capture and Energy Conversion and Storage. *Energy Technol.* **2022**, *10*, 2200498. [CrossRef]
79. Ouyang, L.; Xiao, J.; Jiang, H.; Yuan, S. Nitrogen-Doped Porous Carbon Materials Derived from Graphene Oxide/Melamine Resin Composites for CO₂ Adsorption. *Molecules* **2021**, *26*, 5293. [CrossRef]
80. Wang, Q.; Han, L.; Wang, Y.; He, Z.; Meng, Q.; Wang, S.; Xiao, P.; Jia, X. Conversion of Coal into N-Doped Porous Carbon for High-Performance SO₂ Adsorption. *RSC Adv.* **2022**, *12*, 20640–20648. [CrossRef]
81. Han, W.; Wang, H.; Xia, K.; Chen, S.; Yan, P.; Deng, T.; Zhu, W. Superior Nitrogen-Doped Activated Carbon Materials for Water Cleaning and Energy Storing Prepared from Renewable Leather Wastes. *Environ. Int.* **2020**, *142*, 105846. [CrossRef] [PubMed]
82. Shang, H.; Li, Y.; Liu, J.; Wan, Y.; Feng, Y.; Yu, Y. Preparation of Nitrogen Doped Magnesium Oxide Modified Biochar and Its Sorption Efficiency of Lead Ions in Aqueous Solution. *Bioresour Technol.* **2020**, *314*, 123708. [CrossRef] [PubMed]
83. Xiao, W.; Jiang, X.; Liu, X.; Zhou, W.; Garba, Z.N.; Lawan, I.; Wang, L.; Yuan, Z. Adsorption of Organic Dyes from Wastewater by Metal-Doped Porous Carbon Materials. *J. Clean. Prod.* **2021**, *284*, 124773. [CrossRef]
84. Montazerolghaem, M.; Aghamiri, S.F.; Tangestaninejad, S.; Talaie, M.R. A Metal-Organic Framework MIL-101 Doped with Metal Nanoparticles (Ni & Cu) and Its Effect on CO₂ Adsorption Properties. *RSC Adv.* **2015**, *6*, 632–640. [CrossRef]
85. Qin, W.; Cao, W.; Liu, H.; Li, Z.; Li, Y. Metal-Organic Framework MIL-101 Doped with Palladium for Toluene Adsorption and Hydrogen Storage. *RSC Adv.* **2014**, *4*, 2414–2420. [CrossRef]
86. Ebrahim, A.M.; Bandoz, T.J. Ce(III) Doped Zr-Based MOFs as Excellent NO₂ Adsorbents at Ambient Conditions. *ACS Appl. Mater. Interfaces* **2013**, *5*, 10565–10573. [CrossRef]
87. Kim, T.; Lee, S.K.; Lee, S.; Lee, J.S.; Kim, S.W. Development of Silver Nanoparticle-Doped Adsorbents for the Separation and Recovery of Radioactive Iodine from Alkaline Solutions. *Appl. Radiat. Isot.* **2017**, *129*, 215–221. [CrossRef]
88. Cheng, Z.-L.; Sun, W. Preparation of Nano-CuO-Loaded Halloysite Nanotubes with High Catalytic Activity for Selective Oxidation of Cyclohexene. *Chin. Chem. Lett.* **2016**, *27*, 81–84. [CrossRef]
89. Rahali, S.; Ben Aissa, M.A.; Khezami, L.; Elamin, N.; Seydou, M.; Modwi, A. Adsorption Behavior of Congo Red onto Barium-Doped ZnO Nanoparticles: Correlation between Experimental Results and DFT Calculations. *Langmuir* **2021**, *37*, 7285–7294. [CrossRef]
90. Hu, P.; Wang, S.; Zhuo, Y. Research on CO₂ Adsorption Performances of Metal-Doped (Ca, Fe and Al) MgO. *Sep. Purif. Technol.* **2021**, *276*, 119323. [CrossRef]

91. Kim, T.S.; Song, H.J.; Dar, M.A.; Lee, H.J.; Kim, D.W. Fast Adsorption Kinetics of Highly Dispersed Ultrafine Nickel/Carbon Nanoparticles for Organic Dye Removal. *Appl. Surf. Sci.* **2018**, *439*, 364–370. [[CrossRef](#)]
92. Fronczak, M.; Demby, K.; Strachowski, P.; Strawski, M.; Bystrzejewski, M. Graphitic Carbon Nitride Doped with the S-Block Metals: Adsorbent for the Removal of Methyl Blue and Copper(II) Ions. *Langmuir* **2018**, *34*, 7272–7283. [[CrossRef](#)] [[PubMed](#)]
93. Kim, S.; Cho, S.Y.; Son, K.; Attia, N.F.; Oh, H. A Metal-Doped Flexible Porous Carbon Cloth for Enhanced CO₂/CH₄ Separation. *Sep. Purif. Technol.* **2021**, *277*, 119511. [[CrossRef](#)]
94. Lei, X.; Huang, L.; Liu, K.; Ouyang, L.; Shuai, Q.; Hu, S. Facile One-Pot Synthesis of Hierarchical N-Doped Porous Carbon for Efficient Ibuprofen Removal. *J. Colloid. Interface Sci.* **2021**, *604*, 823–831. [[CrossRef](#)]
95. Lu, S.; Huang, X.; Tang, M.; Peng, Y.; Wang, S.; Makwarimba, C.P. Synthesis of N-Doped Hierarchical Porous Carbon with Excellent Toluene Adsorption Properties and Its Activation Mechanism. *Environ. Pollut.* **2021**, *284*, 117113. [[CrossRef](#)]
96. Wang, R.; Wang, D.; Peng, W.; Zhang, J.; Liu, J.; Wang, Y.; Wang, X. Removal of F[−] from Water by Magnetic Floriform Magnesium Zirconium Hydroxalcalite-like Material Doped with Fe₂O₃ and ZrO₂. *Desalination* **2022**, *544*, 116142. [[CrossRef](#)]
97. Bakry, A.M.; Awad, F.S.; Bobb, J.A.; El-Shall, M.S. Multifunctional Binding Sites on Nitrogen-Doped Carboxylated Porous Carbon for Highly Efficient Adsorption of Pb(II), Hg(II), and Cr(VI) Ions. *ACS Omega* **2020**, *5*, 33090–33100. [[CrossRef](#)]
98. Kamran, U.; Park, S.J. Microwave-Assisted Acid Functionalized Carbon Nanofibers Decorated with Mn Doped TNTs Nanocomposites: Efficient Contenders for Lithium Adsorption and Recovery from Aqueous Media. *J. Ind. Eng. Chem.* **2020**, *92*, 263–277. [[CrossRef](#)]
99. Mukhtar, A.; Saqib, S.; Mellon, N.B.; Rafiq, S.; Babar, M.; Ullah, S.; Muhammad, N.; Khan, A.L.; Ayoub, M.; Ibrahim, M.; et al. A Review on CO₂ Capture via Nitrogen-Doped Porous Polymers and Catalytic Conversion as a Feedstock for Fuels. *J. Clean. Prod.* **2020**, *277*, 123999. [[CrossRef](#)]
100. Sanjabi, A.; Azizian, S.; Torabi, M.; Zolfigol, M.A.; Yarie, M. On the Applicability of Triazine-Based Covalent Organic Polymer as Adsorbent for Dye Removal from Aqueous Solution. *Microporous Mesoporous Mater.* **2023**, *348*, 112367. [[CrossRef](#)]
101. Aliabadi, H.M.; Zargoosh, K. Synthesis of 3-Amino-1,2,4-Triazole-5-Thiol Functionalized p-Phenylenediamine Covalent Organic Polymer as a Highly Selective Adsorbent for Hg₂⁺ Ions. *React. Funct. Polym.* **2023**, *186*, 105575. [[CrossRef](#)]
102. Zolfaghari, S.; Sharafdini, R.; Ghaedi, M.; Javadian, H.; Shokrollahi, A.; Shahvandi, S.K.; Rodrigues, V.H.N.; Razmjoue, D. Synthesis of a Coordination Polymer Based on Zn(DMF)(Tp) as a Novel Adsorbent for the Simultaneous Removal of Quinoline Yellow and Azure B. *J. Mol. Struct.* **2023**, *1294*, 136572. [[CrossRef](#)]
103. Abdelmoaty, Y.H.; Tessema, T.D.; Choudhury, F.A.; El-Kadri, O.M.; El-Kaderi, H.M. Nitrogen-Rich Porous Polymers for Carbon Dioxide and Iodine Sequestration for Environmental Remediation. *ACS Appl. Mater. Interfaces* **2018**, *10*, 16049–16058. [[CrossRef](#)]
104. Qu, J.G.; Li, N.N.; Liu, B.J.; He, J.X. Preparation of BiVO₄/Bentonite Catalysts and Their Photocatalytic Properties under Simulated Solar Irradiation. *Mater. Sci. Semicond. Process.* **2013**, *16*, 99–105. [[CrossRef](#)]
105. Vaiano, V.; Iervolino, G.; Rizzo, L. Cu-Doped ZnO as Efficient Photocatalyst for the Oxidation of Arsenite to Arsenate under Visible Light. *Appl. Catal. B* **2018**, *238*, 471–479. [[CrossRef](#)]
106. Rosa, D.; D'Agostino, F.; Bavasso, I.; Bracciale, M.P.; Di Palma, L. Easy Way to Produce Iron-Doped Titania Nanoparticles via the Solid-State Method and Investigation Their Photocatalytic Activity. *J. Mater. Res.* **2023**, *38*, 1282–1292. [[CrossRef](#)]
107. Xing, M.; Fang, W.; Nasir, M.; Ma, Y.; Zhang, J.; Anpo, M. Self-Doped Ti₃⁺-Enhanced TiO₂ Nanoparticles with a High-Performance Photocatalysis. *J. Catal.* **2013**, *297*, 236–243. [[CrossRef](#)]
108. Chen, Z.; Li, Y.; Guo, M.; Xu, F.; Wang, P.; Du, Y.; Na, P. One-Pot Synthesis of Mn-Doped TiO₂ Grown on Graphene and the Mechanism for Removal of Cr(VI) and Cr(III). *J. Hazard. Mater.* **2016**, *310*, 188–198. [[CrossRef](#)]
109. Jiang, Y.; Chowdhury, S.; Balasubramanian, R. Nitrogen-Doped Graphene Hydrogels as Potential Adsorbents and Photocatalysts for Environmental Remediation. *Chem. Eng. J.* **2017**, *327*, 751–763. [[CrossRef](#)]
110. Hong, S.P.; Kim, S.; Kim, N.; Yoon, J.; Kim, C. A Short Review on Electrochemically Self-Doped TiO₂ Nanotube Arrays: Synthesis and Applications. *Korean J. Chem. Eng.* **2019**, *36*, 1753–1766. [[CrossRef](#)]
111. Zhang, Z.; Hedhili, M.N.; Zhu, H.; Wang, P. Electrochemical Reduction Induced Self-Doping of Ti₃⁺ for Efficient Water Splitting Performance on TiO₂ Based Photoelectrodes. *Phys. Chem. Chem. Phys.* **2013**, *15*, 15637–15644. [[CrossRef](#)]
112. Cao, J.; Yang, Z.-H.; Xiong, W.-P.; Zhou, Y.-Y.; Peng, Y.-R.; Li, X.; Zhou, C.-Y.; Xu, R.; Zhang, Y.-R. One-Step Synthesis of Co-Doped UiO-66 Nanoparticle with Enhanced Removal Efficiency of Tetracycline: Simultaneous Adsorption and Photocatalysis. *Chem. Eng. J.* **2018**, *353*, 126–137. [[CrossRef](#)]
113. Adam, F.A.; Ghoniem, M.G.; Diawara, M.; Rahali, S.; Abdulkhair, B.Y.; Elamin, M.R.; Ben Aissa, M.A.; Seydou, M. Enhanced Adsorptive Removal of Indigo Carmine Dye by Bismuth Oxide Doped MgO Based Adsorbents from Aqueous Solution: Equilibrium, Kinetic and Computational Studies. *RSC Adv.* **2022**, *12*, 24786–24803. [[CrossRef](#)] [[PubMed](#)]
114. Cheng, S.; Zhang, L.; Xia, H.; Peng, J.; Shu, J.; Li, C. Ultrasound and Microwave-Assisted Preparation of Fe-Activated Carbon as an Effective Low-Cost Adsorbent for Dyes Wastewater Treatment. *RSC Adv.* **2016**, *6*, 78936–78946. [[CrossRef](#)]
115. Wang, Y.; Xiao, J.; Wang, H.; Zhang, T.C.; Yuan, S. Binary Doping of Nitrogen and Phosphorus into Porous Carbon: A Novel Di-Functional Material for Enhancing CO₂ Capture and Super-Capacitance. *J. Mater. Sci. Technol.* **2022**, *99*, 73–81. [[CrossRef](#)]
116. Fouda-Mbanga, B.G.; Prabakaran, E.; Pillay, K. Cd²⁺ Ion Adsorption and Re-Use of Spent Adsorbent with N-Doped Carbon Nanoparticles Coated on Cerium Oxide Nanorods Nanocomposite for Fingerprint Detection. *Chem. Phys. Impact* **2022**, *5*, 100083. [[CrossRef](#)]

117. Bhat, S.A.; Zafar, F.; Mirza, A.U.; Mondal, A.H.; Kareem, A.; Haq, Q.M.R.; Nishat, N. NiO Nanoparticle Doped-PVA-MF Polymer Nanocomposites: Preparation, Congo Red Dye Adsorption and Antibacterial Activity. *Arab. J. Chem.* **2020**, *13*, 5724–5739. [[CrossRef](#)]
118. Lather, R.; Jeevanandam, P. Synthesis of Zn³⁺ Doped SnS₂ Nanoparticles Using a Novel Thermal Decomposition Approach and Their Application as Adsorbent. *J. Alloys Compd.* **2022**, *891*, 161989. [[CrossRef](#)]
119. Dadfarnia, S.; Haji Shabani, A.M.; Moradi, S.E.; Emami, S. Methyl Red Removal from Water by Iron Based Metal-Organic Frameworks Loaded onto Iron Oxide Nanoparticle Adsorbent. *Appl. Surf. Sci.* **2015**, *330*, 85–93. [[CrossRef](#)]
120. Li, H.; Tang, M.; Huang, X.; Wang, L.; Liu, Q.; Lu, S. An Efficient Biochar Adsorbent for CO₂ Capture: Combined Experimental and Theoretical Study on the Promotion Mechanism of N-Doping. *Chem. Eng. J.* **2023**, *466*, 143095. [[CrossRef](#)]
121. Guaya, D.; Jiménez, R.; Sarango, J.; Valderrama, C.; Cortina, J.L. Iron-Doped Natural Clays: Low-Cost Inorganic Adsorbents for Phosphate Recovering from Simulated Urban Treated Wastewater. *J. Water Process Eng.* **2021**, *43*, 102274. [[CrossRef](#)]
122. Naskar, A.; Khan, H.; Jana, S. One Pot Low Temperature Synthesis of Graphene Coupled Gd-Doped ZnFe₂O₄ Nanocomposite for Effective Removal of Antibiotic Levofloxacin Drug. *J. Solgel Sci. Technol.* **2018**, *86*, 599–609. [[CrossRef](#)]
123. Ma, J.; Zhang, M.; Ji, M.; Zhang, L.; Qin, Z.; Zhang, Y.; Gao, L.; Jiao, T. Magnetic Graphene Oxide-Containing Chitosan-sodium Alginate Hydrogel Beads for Highly Efficient and Sustainable Removal of Cationic Dyes. *Int. J. Biol. Macromol.* **2021**, *193*, 2221–2231. [[CrossRef](#)] [[PubMed](#)]
124. Kong, L.; Yan, Q.; Wang, Y.; Wang, Q.; Andrews, C.B.; Zheng, C. Self-Supported Trimetallic NiZnLa Nanosheets on Hierarchical Porous Graphene Oxide-Polymer Composite Fibers for Enhanced Phosphate Removal from Water. *J. Colloid. Interface Sci.* **2022**, *628*, 807–818. [[CrossRef](#)] [[PubMed](#)]
125. Fang, Z.B.; Liu, T.T.; Liu, J.; Jin, S.; Wu, X.P.; Gong, X.Q.; Wang, K.; Yin, Q.; Liu, T.F.; Cao, R.; et al. Boosting Interfacial Charge-Transfer Kinetics for Efficient Overall CO₂ Photoreduction via Rational Design of Coordination Spheres on Metal-Organic Frameworks. *J. Am. Chem. Soc.* **2020**, *142*, 12515–12523. [[CrossRef](#)] [[PubMed](#)]
126. Cao, Z.; Qin, M.; Gu, Y.; Jia, B.; Chen, P.; Qu, X. Synthesis and Characterization of Sn-Doped Hematite as Visible Light Photocatalyst. *Mater. Res. Bull.* **2016**, *77*, 41–47. [[CrossRef](#)]
127. Albukhari, S.M.; Ismail, A.A. Highly Dispersed Pt Nanoparticle-Doped Mesoporous ZnO Photocatalysts for Promoting Photoconversion of CO₂ to Methanol. *ACS Omega* **2021**, *6*, 23378–23388. [[CrossRef](#)]
128. Singh, R.; Ladol, J.; Khajuria, H.; Nawaz Sheikh, H. Nitrogen Doped Graphene Nickel Ferrite Magnetic Photocatalyst for the Visible Light Degradation of Methylene Blue. *Acta Chim. Slov.* **2017**, *64*, 170–178. [[CrossRef](#)]
129. Lavorato, C.; Primo, A.; Molinari, R.; Garcia, H. N-Doped Graphene Derived from Biomass as a Visible-Light Photocatalyst for Hydrogen Generation from Water/Methanol Mixtures. *Chem.-A Eur. J.* **2014**, *20*, 187–194. [[CrossRef](#)]
130. Velu, M.; Balasubramanian, B.; Velmurugan, P.; Kamyab, H.; Ravi, A.V.; Chelliapan, S.; Lee, C.T.; Palaniyappan, J. Fabrication of Nanocomposites Mediated from Aluminium Nanoparticles/Moringa Oleifera Gum Activated Carbon for Effective Photocatalytic Removal of Nitrate and Phosphate in Aqueous Solution. *J. Clean. Prod.* **2021**, *281*, 124553. [[CrossRef](#)]
131. Zhang, Y.; Chen, Y.; Hei, Y.; Wang, S.; Shi, Y.; Jiang, F.; Luo, L. Design and Controllable Synthesis of C-Doped Bi₂O₃ Nanowires with Superior Performance for Removal of Bisphenol A. *Mater. Sci. Semicond. Process.* **2021**, *132*, 105875. [[CrossRef](#)]
132. Nguyen, L.T.T.; Nguyen, H.T.T.; Nguyen, L.T.H.; Duong, A.T.T.; Nguyen, H.Q.; Ngo, V.T.M.; Vu, N.V.; Nguyen, D.T.C.; Tran, T. Van Efficient and Recyclable Nd³⁺-Doped CoFe₂O₄ for Boosted Visible Light-Driven Photocatalytic Degradation of Rhodamine B Dye. *RSC Adv.* **2023**, *13*, 10650–10656. [[CrossRef](#)] [[PubMed](#)]
133. Yahya, N.; Aziz, F.; Jamaludin, N.; Mutalib, M.A.; Ismail, A.; Salleh, W.W.; Jaafar, J.; Yusof, N.; Ludin, N.A. A Review of Integrated Photocatalyst Adsorbents for Wastewater Treatment. *J. Environ. Chem. Eng.* **2018**, *6*, 7411–7425. [[CrossRef](#)]
134. Xu, J.; Ao, Y.; Fu, D.; Yuan, C. Synthesis of Fluorine-Doped Titania-Coated Activated Carbon under Low Temperature with High Photocatalytic Activity under Visible Light. *J. Phys. Chem. Solids* **2008**, *69*, 2366–2370. [[CrossRef](#)]
135. Belver, C.; Bedia, J.; Rodriguez, J.J. Zr-Doped TiO₂ Supported on Delaminated Clay Materials for Solar Photocatalytic Treatment of Emerging Pollutants. *J. Hazard. Mater.* **2017**, *322*, 233–242. [[CrossRef](#)]
136. Bian, Z.; Feng, Y.; Li, H.; Yu, H.; Wu, H. Adsorption-Photocatalytic Degradation and Kinetic of Sodium Isobutyl Xanthate Using the Nitrogen and Cerium Co-Doping TiO₂⁻ Coated Activated Carbon. *Chemosphere* **2021**, *263*, 128254. [[CrossRef](#)]
137. Wang, T.; Dissanayake, P.D.; Sun, M.; Tao, Z.; Han, W.; An, N.; Gu, Q.; Xia, D.; Tian, B.; Ok, Y.S.; et al. Adsorption and Visible-Light Photocatalytic Degradation of Organic Pollutants by Functionalized Biochar: Role of Iodine Doping and Reactive Species. *Environ. Res.* **2021**, *197*, 111026. [[CrossRef](#)]
138. Henych, J.; Št'astný, M.; Němečková, Z.; Kormunda, M.; Šanderová, Z.; Žmudová, Z.; Ryšánek, P.; Stehlík, Š.; Ederer, J.; Liegertová, M.; et al. Cerium-Bismuth Oxides/Oxynitrates with Low Toxicity for the Removal and Degradation of Organophosphates and Bisphenols. *ACS Appl. Nano Mater.* **2022**, *5*, 17956–17968. [[CrossRef](#)]
139. Primo, A.; Corma, A.; García, H. Titania Supported Gold Nanoparticles as Photocatalyst. *Phys. Chem. Chem. Phys.* **2011**, *13*, 886–910. [[CrossRef](#)]
140. Oladoye, P.O.; Adegboyega, S.A.; Giwa, A.R.A. Remediation Potentials of Composite Metal-Organic Frameworks (MOFs) for Dyes as Water Contaminants: A Comprehensive Review of Recent Literatures. *Environ. Nanotechnol. Monit. Manag.* **2021**, *16*, 100568. [[CrossRef](#)]

141. Dong, H.; Zeng, G.; Tang, L.; Fan, C.; Zhang, C.; He, X.; He, Y. An Overview on Limitations of TiO₂-Based Particles for Photocatalytic Degradation of Organic Pollutants and the Corresponding Countermeasures. *Water Res.* **2015**, *79*, 128–146. [[CrossRef](#)] [[PubMed](#)]
142. Cheng, R.; Xia, J.; Wen, J.; Xu, P.; Zheng, X. Nano Metal-Containing Photocatalysts for the Removal of Volatile Organic Compounds: Doping, Performance, and Mechanisms. *Nanomaterials* **2022**, *12*, 1335. [[CrossRef](#)] [[PubMed](#)]
143. Barua, A.; Mehra, P.; Paul, A. Role of Nitrogen Doping and Pore Volume for CO₂ Capture in Metal-Organic Framework Derived Ultramicroporous Carbon Material. *Results Chem.* **2023**, *5*, 100807. [[CrossRef](#)]

Disclaimer/Publisher's Note: The statements, opinions and data contained in all publications are solely those of the individual author(s) and contributor(s) and not of MDPI and/or the editor(s). MDPI and/or the editor(s) disclaim responsibility for any injury to people or property resulting from any ideas, methods, instructions or products referred to in the content.